A SINGLE-DEGREE-OF-FREEDOM MODEL FOR NON-LINEAR SOIL AMPLIFICATION

by

Mustafa O. Erdik

UNITED STATES
DEPARTMENT OF THE INTERIOR
GEOLOGICAL SURVEY

Open-File Report
79-592

March 1979

Menlo Park, California

This page intentionally left blank

CONTENTS

INTRODUCTION

For proper understanding of soil behavior during earthquakes and assessment of a realistic surface motion, studies of the large-strain dynamic response of non-linear hysteretic soil systems are indispensable. Most of the presently available studies are based on the assumption that the response of a soil deposit is mainly due to the upward propagation of horizontally polarized shear waves from the underlying bedrock. Equivalent-linear procedures, currently in common use in non-linear soil response analysis, provide a simple approach and have been favorably compared with the actual recorded motions in some particular cases. In this regard, Idriss and Seed (1968); Seed and Idriss (1969); Schnabel et al (1972) should be mentioned. Strain compatibility in these equivalent-linear approaches is maintained by selecting values of shear moduli and damping ratios in accordance with the average soil strains, in an iterative manner. Truly non-linear constitutive models with complete strain compatibility have also been employed (Cervantes et al. (1973), Constantopulos (1973), Papadakis (1973), Faccioli et al. (1973), Streeter et al (1974) and Joyner and Chen (1975).

The equivalent-linear approaches often raise some doubt as to the reliability of their results concerning the system response in high frequency regions. Through the use of a truly non-linear model, Joyner and Chen (1975) have shown that in these frequency regions the equivalent-linear methods may underestimate the surface motion by as much as a factor of two or more.

Although these aforementioned studies are complete in their methods of analysis, they inevitably provide applications pertaining only to a few specific soil systems, and do not lead to general conclusions about soil behavior.

This report attempts to provide a general picture of the soil response

through the use of a single-degree-of-freedom non-linear-hysteretic model. Although the investigation is based on a specific type of nonlinearity and a set of dynamic soil properties, the method described does not limit itself to these assumptions and is equally applicable to other types of nonlinearity and soil parameters.

DESCRIPTION OF THE SOIL LAYER AND PROPERTIES

This report considers the responses associated with the vertical propagation of SH waves through a non-linear hysteretic soil layer as shown in Fig. 1. The layer rests on a rigid bedrock half-space and the soil layer-bedrock system is assumed to extend to infinity in the horizontal directions.

Dynamic properties of soil layers have been investigated for various soil types, e.g., Bishop, et al (1961), Hardin and Black (1969), Dobry (1970), Ladd and Edgers (1972), Hardin and Drnevich (1972 a,b), Richart (1975). These studies indicate that the Masing hypothesis (Masing, 1926) is satisfied and, by an appropriate choice of parameters, the constitutive model shown in Fig. 2 can closely fit the dynamic behavior of real soils. In this report, the dynamic soil parameters will be determined by the methods of Hardin and Drnevich (1972 b).

The key parameters are the maximum shear stress τ_{max}, and the low strain shear modulus G_{max}. On the basis of these parameters the initial loading curve of stress, τ, against strain, γ, can be approximated by

$$\frac{\tau}{\tau_{max}} = \frac{\frac{\gamma}{\gamma_r}}{\frac{\gamma}{\gamma_r} + 1} \qquad (1)$$

where

$$\gamma_r = \frac{\tau_{max}}{G_{max}} \tag{2}$$

is called the reference strain. Denoting $\frac{\tau}{\tau_{max}}$ by s, and $\frac{\gamma}{\gamma_r}$ by ε the non-linear constitutive relation can be given as follows:

Initial loading curve: $s = \frac{\varepsilon}{\varepsilon + 1}$ (3)

Unloading path : $s = \frac{2(\varepsilon - \varepsilon_o)}{\varepsilon - \varepsilon_o + 2} + s_o$ (4)

Reloading path : $s = \frac{2(\varepsilon + \varepsilon_o)}{\varepsilon + \varepsilon_o + 2} - s_o$ (5)

Where s_o and ε_o are respectively the absolute values of the normalized stress and strain at the initiation of unloading and reloading under cyclic loading conditions.

For the unloading and reloading paths the constitutive equations are simplified if the origin of the coordinate system is transferred to the points of unloading and reloading respectively and will take the following form:

$$s = \frac{2\varepsilon}{\varepsilon+2} \tag{6}$$

Variation of G_{max} through the depth of layer, H, for many undisturbed cohesive soils, as well as sands, can be expressed as:

$$G_{max} = C_m \, \overline{\sigma}_m^{1/2} \, (OCR)_m^K \tag{7}$$

Where, $\overline{\sigma}_m$ is the mean principal effective stress and $(OCR)_m$ is the overconsolidation ratio in terms of the mean effective principal stresses. C_m and K are constants depending on the void ratio, e , and the plasticity index, P.I. respectively.

It is more convenient to work with the vertical stress rather than mean stress. The relationship between the mean principal effective stress $\overline{\sigma}_m$, and the vertical effective stress, $\overline{\sigma}_v$, can be given in terms of the coefficient of earth pressure at rest, K_o. Values of K_o are provided for cohesive soils as a function of plasticity index and OCR, (or effective angle of internal friction and OCR) by Brooker and Ireland (1965). Analysis of these data suggests that G_{max} can be given in terms of the vertical effective stresses as

$$G_{max} = C_G \overline{\sigma}_v^{1/2} (OCR)^{K+K'} \tag{8}$$

where exponent K' is a function of the plasticity index or effective angle of internal friction. In the rest of this study (K + K') will be represented by a single variable , Q.

For the maximum shear stress ,τ_{max}, Hardin and Drnevich (1972a) provide the following expression for normally consolidated soils:

$$\tau_{max} = \left\{ \left[\frac{1+K_o}{2} \overline{\sigma}_v \sin\bar{\phi} + \bar{c}\cos\bar{\phi} \right]^2 - \left[\frac{1-K_o}{2} \overline{\sigma}_v \right]^2 \right\}^{1/2} \tag{9}$$

where $\bar{\phi}$ is the angle of shearing resistance and $\bar{c}$ is the cohesion, both in terms of the effective stresses. By assuming that the cohesion, $\bar{c}$, is

zero for normally consolidated materials Eq. 9 can be written as follows:

$$\tau_{max} = C_s \bar{\sigma}_v \tag{10}$$

where

$$C_s = \left[\left(\frac{1+K_o}{2} \sin \bar{\phi} \right)^2 - \left(\frac{1-K_o}{2} \right)^2 \right]^{1/2} \tag{11}$$

Analysis of the data provided by Ladd and Edgers (1972) for five different clays (Fig. 3) indicate that for overconsolidated cohesive soils τ_{max} can be approximated as:

$$\tau_{max} = C_s \bar{\sigma}_v (OCR)^T \tag{12}$$

within the range of overconsolidation ratios equal to 1 and 10.

METHOD OF ANALYSIS

General

An analogous single-degree-of-freedom (SDF) model representing the first mode characteristics of the actual multi-degree-of-freedom (MDF) soil layer can be derived by setting the natural frequency of the SDF system equal to the first modal frequency of the soil layer and by insuring that for all strain levels the amount of energy dissipated per cycle by the SDF model is equal to the amount dissipated by the soil layer responding in its first mode. For nonlinear systems responding in small but non-zero strain levels the term frequency applies to the apparent frequency of vibration. For non-linearities of the type considered, the apparent frequency of vibration in the small but non-zero ranges of strain can be satisfactorily approximated by employing the secant modulus of shear, G, corresponding to these strain ranges instead of the initial tangent modulus, G_{max}. G and G_{max} are indicated on Fig. 2 for illustration.

Theory

The equation of shear vibration of a soil column of unit cross sectional area is:

$$\frac{\partial\left(G_{max}\frac{\partial u}{\partial z}\right)}{\partial z} = \rho\frac{\partial^2 u}{\partial t^2} \qquad (13)$$

Where u denotes the lateral displacement, z is the depth measured along the vertical axis, and ρ is the mass density. (Fig. 1).

For a soil layer vibrating in its r^{th} mode, with a circular frequency of ω_r:

$$u(z,t) = u_r(z) \sin \omega_r t \tag{14}$$

where $u_r(z)$ is the rth mode shape.

substituting into Eq. (13) and separating the variables

$$\frac{d\left(G_{max} \frac{du_r}{dz}\right)}{dz} = \rho \omega_r^2 u_r \tag{15}$$

and

$$u_r(z) = \omega_r^2 \int_0^z \frac{1}{G_{max}(y)} \int_0^y \rho(x)\, u_r(x)\, dx\, dy \tag{16}$$

subject to the boundary conditions of

(zero stress) $$\frac{du_r}{dz} = 0 \quad \text{at} \quad z = 0 \tag{17}$$

(zero displacement) $$u_r(H) = 0 \quad \text{at} \quad z = H \tag{18}$$

Application of these boundary conditions to Eq. 16 results in the following integral equation:

$$\frac{1}{\omega_r^2} u_r(z) = \int_0^z \frac{1}{G_{max}(y)} \int_0^y \rho(x)\, u_r(x)\, dx\, dy - \int_0^H \frac{1}{G_{max}(y)} \int_0^y \rho(x)\, u_r(x)\, dx\, dy \tag{19}$$

Solution of this integral equation will lead to the modal displacements and frequencies. To obtain the first modal properties the Stodola-Vianella procedure (Stodola 1927) will be employed. In this iterative procedure first a trial function $u_1^{(1)}$, satisfying the boundary conditions and resembling the first modal shape is selected. This function is placed in the integrand of Eq. 19 and the integration is performed yielding a new function $u_1^{(2)}$. This function is, in turn, inserted in the integrand and integrated again, this time to yield $u_1^{(3)}$. Through the use of orthogonality of modes it can be shown that the elements of the true first mode present in the trial function will consecutively be amplified, and the functions obtained through this iteration will converge to a multiple of the first mode (Hurty and Rubinstein, 1964). At any iteration step the ratio ($u_1^{(i-1)} / u_1^{(i)}$) can be used to approximate the first modal circular frequency ω_1 within the integration domain. Through the use of "enclosure theorem" (Crandall, 1956) it can be shown that the true frequency will lie between the extremum values within the integration domain. A very good approximation of ω_1 can be obtained by employing the following "Schwarz Quotient" based on the least squares minimization of the residuals (Crandall 1956).

$$\omega_1^2 = \frac{\int_0^H \left[u_1^{(i-1)}\right]^2 dz}{\int_0^H u_1^{(i-1)}\, u_1^{(i)}\, dz} \tag{20}$$

Although $u_1^{(1)}(z) = \cos\frac{\pi}{2}\frac{z}{H}$ seems an obvious choice for the first trial function for Eq. (19), it is not suited for explicit integration since it leads to Fresnel integrals with numerical solutions only. A satisfactory choice for the first trial function can be taken as:

$$u_1^{(1)}(z) = u_0\left[1 - \left(\frac{z}{H}\right)^2\right] \tag{21}$$

where u_0 is the displacement at the surface. From Eq. 8, neglecting the overconsolidated part of the soil layer, the initial tangent modulus of rigidity can be written as:

$$G_{max} = K_2 z^{1/2} \tag{22}$$

K_2 is a constant for a given soil layer. Assuming constant mass density throughout the soil layer:

$$\rho(z) = \rho \tag{23}$$

Substituting Eqs. 21, 22, and 23 into Eq. 19 and carrying out two consecutive iterations the following approximations of the first modal displacement can be obtained:

$$u_1^{(2)} = u_0\left[1 + \frac{1}{6}\left(\frac{z}{H}\right)^{7/2} - \frac{7}{6}\left(\frac{z}{H}\right)^{3/2}\right] \tag{24}$$

and

$$u_1^{(3)} = u_0\left[1 - \frac{4}{280}\left(\frac{z}{H}\right)^{5} + \frac{84}{280}\left(\frac{z}{H}\right)^{3} - \frac{360}{280}\left(\frac{z}{H}\right)^{3/2}\right] \tag{25}$$

Using Eqs. 24 and 25 in the Schwartz Quotient one can obtain the first circular frequency of vibration as:

$$\omega_1^2 = \frac{\overline{G}_{max}}{0.3402\rho H^2} \tag{26}$$

where

$$\overline{G}_{max} = \frac{1}{H} \int_0^H G_{max}\, dz \tag{27}$$

is the average tangent modulus of rigidity along the soil column. Eq. 26 compares exactly with the results reported by Dobry et al. (1971) and (1976). Note that all of the Eqs. 24, 25 and 26 are valid under the assumption that the soil exhibits very small strains or, in other words, responds in the so-called linear ranges of deformation. Substituting G, the secant modulus of rigidity, instead of G_{max}, the initial tangent modulus of rigidity in Eq. 19, carrying out the indicated iterations, and using the Schwarz Quotient, we will try to approximate the strain-dependent first mode characteristics of the soil layer.

From the definition of secant modulus of rigidity, the following equation can be derived.

$$G = \frac{\tau}{\gamma} = \frac{G_{max}\,\tau_{max}}{\tau_{max} + \gamma G_{max}} \tag{28}$$

Substituting Eq. 22 for G_{max}, and Eq. 29 for τ_{max};

$$\tau_{max} = K_1 z \tag{29}$$

where K_1 is a constant for a given soil layer, and using the gradient of Eq. 21, given by Eq. 30, to approximate γ,

$$\gamma = \left| \frac{du}{dz} \right| = 2 \frac{u_o}{H} \frac{z}{H} \tag{30}$$

Eq. 28 takes the following form:

$$G = \frac{\overline{G}_{max} \left(\frac{z}{H}\right)^{1/2}}{\frac{2}{3} + \left(\frac{u_o}{H} \frac{\overline{G}_{max}}{\overline{\tau}_{max}}\right)\left(\frac{z}{H}\right)^{1/2}} \tag{31}$$

where

$$\overline{\tau}_{max} = \frac{1}{H} \int_0^H \tau_{max} \, dz \tag{32}$$

is the average maximum shear stress along the soil column.

Define a "reference displacement", U_r (analogous to the reference strain, γ_r) as the surface displacement obtained by integration of the reference strain throughout the depth of the soil layer, given by the following equation.

$$\Delta J_r = \int_0^H \gamma_r \, dz \tag{33}$$

Upon substituting Eq. 2 for γ_r together with Eqs. 22 and 29

$$\gamma_r = \frac{4}{3} \frac{\overline{\tau}_{max}}{\overline{G}_{max}} \left(\frac{z}{H}\right)^{1/2} \tag{34}$$

and integrating, U_r can be given as:

$$U_r = \frac{8}{9} H \frac{\overline{\tau}_{max}}{\overline{G}_{max}} \tag{35}$$

Substitution of Eq. 35 into Eq. 31 yields:

$$G = \overline{G}_{max} \frac{\left(\frac{z}{H}\right)^{1/2}}{2/3 + 8/9 \frac{u_o}{\Delta J_r} \left(\frac{z}{H}\right)^{1/2}} \tag{36}$$

Eq. 36 approximates the secant modulus of rigidity in terms of the surface

displacement normalized with respect to the reference displacement. Eq. 19 can be written in terms of secant modulus of rigidity by replacing G_{max} with G given by Eq. 36. Using Eq. 21 as the first trial function in the integrand and iterating once:

$$u_1^{(2)} = \frac{u_o}{1 + \frac{35}{36}\frac{u_o}{\Gamma_r}} \left\{ \left[1 - \frac{7}{6}\left(\frac{z}{H}\right)^{3/2} + \frac{1}{6}\left(\frac{z}{H}\right)^{7/2} \right] + \frac{u_o}{\Gamma_r}\left[\frac{35}{36} - \frac{7}{6}\left(\frac{z}{H}\right)^2 + \frac{7}{36}\left(\frac{z}{H}\right)^4 \right] \right\} \tag{37}$$

can be obtained. Note that for the limiting case of $\frac{u_o}{\Gamma_r}$ approaching zero Eq. 37 converges to Eq. 24 as expected.

Through the use of the Schwarz Quotient, employing Eqs. 21 and 37, the following first modal apparent frequency, $(\omega_1)_a$, can be obtained:

$$(\omega_1^2)_a = \frac{\overline{G}_{max}}{0.3362\, \rho H^2 \left[1 + 1.07 \frac{u_o}{\Gamma_r} \right]} \tag{38}$$

or

$$(\omega_1^2)_a = \omega_1^2 \frac{1}{1 + 1.07 \frac{u_o}{\Gamma_r}} \tag{39}$$

where ω_1^2 is given by Eq. 26. Eq. 39 is a first order approximation of the relation between the apparent frequency and the small strain fundamental frequency of the soil layer.

Energy Dissipated Per Hysteresis Cycle

The area bounded by the unloading and reloading paths in Fig. 2 is equal to the energy dissipated, e, by an infinitesimal soil element going through one complete hysteresis cycle with a normalized strain amplitude, ε, and is given by:

$$e = 2\tau_{max}\gamma_r \left[\int_0^{2\varepsilon} \frac{2\eta\, d\eta}{\eta+2} - \frac{1}{2}(2\varepsilon)\frac{2(2\varepsilon)}{(2\varepsilon)+2} \right] \qquad (40)$$

where η is a dummy variable. Carrying out the integration the following equation is obtained:

$$e = \tau_{max}\gamma_r \left[8\varepsilon - 8\ln(\varepsilon+1) - \frac{4\varepsilon^2}{\varepsilon+1} \right] \qquad (41)$$

The normalized strain, ε, is given by $= \frac{\gamma}{\gamma_r}$. Replacing γ by

$$\gamma = \frac{du_1^{(2)}}{dz} \qquad (42)$$

where $u_1^{(2)}$ is given by Eq. 37, and replacing γ_r by Eq. 34 together with Eq. 35, ε can be obtained as:

$$\varepsilon = \frac{\frac{3}{2}\frac{u_o}{U_r}}{1+\frac{35}{36}\frac{u_o}{U_r}} \left\{ -\frac{7}{4} + \frac{7}{12}\left(\frac{z}{H}\right)^2 + \frac{u_o}{U_r}\left[-\frac{7}{3}\left(\frac{z}{H}\right)^{1/2} + \frac{7}{9}\left(\frac{z}{H}\right)^{5/2} \right] \right\} \tag{43}$$

Through the use of Eq. 29, 32, 34 and 35, $\tau_{max}\gamma_r$ can be given as:

$$\tau_{max}\gamma_r = \frac{3}{H} U_r \bar{\tau}_{max} \left(\frac{z}{H}\right)^{3/2} \tag{44}$$

The total energy lost by the soil layer E_{soil} going through a complete cycle of oscillation, equals to the integral of Eq. 40 throughout the depth of layer.

$$E_{soil} = U_r \bar{\tau}_{max} \int_0^1 3\left(\frac{z}{H}\right)^{3/2} \left[8\varepsilon - 8\ln(\varepsilon+1) - \frac{4\varepsilon^2}{\varepsilon+1} \right] d\left(\frac{z}{H}\right) \tag{45}$$

where ε is given by Eq. 43. For a given $\frac{u_o}{U_r}$ the above equation can be numerically integrated to obtain $\frac{E_{soil}}{U_r \tau_{max}}$. Integration results are shown in Table 1, for representative values of $\frac{u_o}{U_r}$.

Analogous Single-Degree-of-Freedom Model

Although the actual determination of the analogous SDF model involved

some trial-and-error procedures, for purposes of presentation the model will be directly proposed and then tested to see how closely it resembles the first modal characteristics of the soil layer.

Let y denote the mass displacement and F denote the spring force of a simple SDF system consisting of a mass, M, and a nonlinear hysteretic spring. The constitutive characteristics of the spring satisfy the Masing hypothesis and are given by the following set of equations.

Initial loading path (Virgin Curve)

$$\frac{F}{F_r} = \frac{\frac{y}{U_r}}{1 + 1.07 \frac{y}{U_r}} \tag{46}$$

Unloading or reloading path

$$\frac{F}{F_r} = \frac{2 \frac{y}{U_r}}{2 + 1.07 \frac{y}{U_r}} \tag{47}$$

where the origin of the coordinate system is transferred to the respective points of unloading and reloading.

In Eq. 46 and 47 U_r is the same reference displacement used in mathematical modeling of the soil layer, and F_r is the reference spring force given by the following equation:

$$F_r = 1.25\,\bar{\tau}_{max} \tag{48}$$

The energy lost by hysteresis in one complete oscillation cycle of the analogous SDF system, E_{SDF}, can be determined as follows:

$$E_{SDF} = 2F_r U_r \left[\int_0^{2\frac{y}{U_r}} \frac{2h\,dh}{2+1.07h} - \frac{2\left(\frac{y}{U_r}\right)^2}{1+1.07\frac{y}{U_r}} \right] \tag{49}$$

or upon carrying out the integration and employing Eq. 48:

$$E_{SDF} = U_r \bar{\tau}_{max} \left\{ \frac{10\frac{y}{U_r}}{1.07} - \frac{10\ln\left[1.07\frac{y}{U_r}+1\right]}{(1.07)^2} - \frac{5\left(\frac{y}{U_r}\right)^2}{1+1.07\left(\frac{y}{U_r}\right)} \right\} \tag{50}$$

Values of $\frac{E_{SDF}}{U_r \bar{\tau}_{max}}$ computed on the basis of Eq. 50 are given in Table 2 for representative values of $\frac{y}{U_r}$.

Comparison of Table 1 and 2 reveals that if y, the SDF mass displacement, is taken equal to u_o, the soil surface displacement, the respective energies dissipated by the soil and SDF systems in an hysteresis cycle will be

approximately equal to each other for all ranges of deformation, or quantitatively speaking, the two energies will not differ from each other, by more than 10% of their respective values.

The initial tangent stiffness, K_{max}, of the analogous SDF system can be obtained from the constitutive relation for the initial loading path as follows:

$$K_{tan} = \frac{dF}{dy} = \frac{F_r}{U_r} \frac{1}{\left[1+1.07\frac{y}{U_r}\right]^2} \tag{51}$$

$$K_{max} = K_{tan}\Big|_{\frac{y}{U_r}=0} = \frac{F_r}{U_r} \tag{52}$$

The secant stiffness, K, is given by the following equation:

$$K = \frac{F}{y} = \frac{F_r}{U_r} \frac{1}{1+1.07\frac{y}{U_r}} \tag{53}$$

The square of the small amplitude frequency of vibration, $(\omega_{SDF})_i$, of an SDF system is directly proportional to the initial tangent stiffness, K_{max}. Assuming that the large amplitude apparent frequency of vibration, $(\omega_{SDF})_a$, can be approximated on the basis of the secant stiffness, K, thus making $(\omega_{SDF})_a^2$ directly proportional to K, the ratio of the apparent frequency of vibration to the small amplitude frequency of vibration

of the analogous SDF system can be given by the following equation:

$$\frac{(\omega_{SDF})_a^2}{(\omega_{SDF})_i^2} = \frac{1}{1 + 1.07 \frac{y}{U_r}} \tag{54}$$

which can be seen to be identical to Eq. 39 if y is taken analogous to u_o

In summary, the SDF system described by the constitutive relations given by Eqs. 46 and 47 satisfies the first modal energy dissipation and frequency characteristics of the soil layer, and the mass displacement of the SDF system is analogous to the surface displacement of the soil layer, provided that the reference displacement and the small amplitude frequency of the analogous SDF system are set equal to those of the soil layer.

Note that this analogy is derived on the basis of the free vibrational properties of the soil layer and the SDF system, where the absolute and relative displacements of the mass are the same. However, for vibrations caused by seismic excitation, distinction should be made between the absolute, y_{ABS}, and the relative, y_{REL}, SDF mass displacements. y_{ABS} and y_{REL} are analogous, respectively, to the absolute and relative surface displacements of the soil layer. The absolute equations of motion of the SDF system can be given as follows:

$$\ddot{y}_{ABS} + \omega_{SDF}^2 y_{ABS} = \omega_{SDF}^2 x_g \tag{55}$$

where ω_{SDF} is the frequency computed on the basis of the tangential stiffness corresponding to the relative displacement history of the mass, and x_g denotes the seismic base displacement.

For the initial loading: ω_{SDF} can be given by utilizing Eq. 39.

$$\omega_{SDF} = (\omega_{SDF})_i \frac{1}{\left[1 + 1.07 \frac{y_r}{U_r}\right]^{1/2}} \tag{56}$$

Similarly, after unloading and reloading:

$$\omega_{SDF} = (\omega_{SDF})_i \frac{4}{\left[2 + 1.07 \frac{|y_r - (y_r)_o|}{U_r}\right]^{1/2}} \tag{57}$$

Where $(y_r)_o$ is the relative mass displacement at the initiation of unloading and/or reloading and $(\omega_{SDF})_i$ is the initial small amplitude frequency taken equal to that of the soil layer, ω_1 .

For a given soil layer U_r can simply be computed through the use of Eq. 33. If the soil layer conforms with the assumptions made in the derivation of Eq. 26 for ω_1, this equation can be employed in determining ω_1 or $(\omega_{SDF})_i$. For any other soil layer, use of discrete Stodola Vianello procedure is recommended (Crandall, 1956). A good study of computational procedures for $(\omega_{SDF})_i$ can be found in Dobry, et al (1976).

Response of the soil layer due to an earthquake excitation from bedrock is obtained by numerical integration of the equations of motion given by Eq. 55. The numerical integration formulae employed assume that the acceleration of the mass during each integration time interval varies linearly and are obtained from Newmark's β-formulae (Newmark, 1959) by taking $\alpha = 1/2$ and $\beta = 1/6$. To increase the speed and efficiency of the integration, the method of direct iteration with no in-step iteration (Erdik, 1975) is used.

COMPARISON WITH A MULTI-DEGREE-OF-FREEDOM ANALYSIS

Some specific solutions obtained on the basis of the proposed single-degree-of-freedom model are compared to those obtained by the multi-degree-of-freedom analysis method of Joyner and Chen (1975). For this purpose, two drastically different soil systems and base rock motions are employed.

The first test case involves a 25 m deep fully saturated soil layer of constant density of 2 gr/cm^3 resting above a rigid bedrock (Joyner, 1977). For simplicity of presentation it is assumed that the soil layer is normally consolidated throughout. G_{max} and τ_{max} are to be computed from Equations 4.1 and 5.1 using:

$$C_G = 0.9 \cdot 10^6 \left(dyn/cm^2\right)^{1/2}$$

and $$C_s = 0.33$$

which are representative values for alluvium in the San Francisco Bay Area.

The input motion, specified at the soil-bedrock interface, is a half-cycle-velocity-pulse that corresponds to an acceleration of consecutive positive and negative triangular spikes of amplitude 0.5 g and duration 0.2 sec. as shown in Fig. 4.

Through the use of Eq. 26 and Eq. 35 the soil layer parameters ω_1 and U_r needed for SDF model can be found as follows:

ω_1=14.406 or f_1 = 2.29 Hz.

and U_r=0.9565 cm.

In both methods of analysis the ground motion is digitized at intervals of 0.01 secs. and the same interval is also used for numerical integration. Results of the surface acceleration and velocity obtained from both methods of analysis are presented in Figs. 5, 6, 7 and 8 for comparison.

The second test case involves the soil profile representing a 200-m section of firm alluvium consisting of predominantly cohesive material. A detailed treatment of the profile characterisics can be found in Joyner and Chen (1975). A constant density of 2.05 gr/cm^3 and a past consolidation vertical stress of 2.94 bars is taken. The material is assigned a plasticity index of 20%, and complete water saturation is presumed at all depths. Coefficients in Eq. 8 and 12 are determined to be:

$$C_G = 0.9 \times 10^6 \left(dyn/cm^2\right)^{1/2}$$

$$K+K' = Q = 0.28$$

$$C_s = 0.33$$

$$T = 0.75$$

To determine the SDF model parameters applicable to such a soil profile, the soil profile is discretized at 10 points and the first small amplitude

frequency of vibration is obtained by employing the discrete Stodola-Vianello method (Newmark and Rosenblueth, 1971; Crandall, 1956). To determine the reference displacement, the constant reference strain value for each discrete step is converted to the reference displacement associated with that step and then summed for all the discrete steps. The SDF model parameters thus determined are:

$$f_1 = 0.499 \text{ Hz}$$

$$U_r = 22.68$$

The input motion prescribed at the soil-bedrock interface is taken to be the first 20 secs. of the N21E component of the Taft strong motion record of the 1952 Kern County, California earthquake. The base acceleration is multiplied by a factor of four, producing a peak acceleration of 0.7 g and a peak velocity of 67 cm/sec, in order to emphasize the effects of nonlinearity and to produce a higher degree of severity for the comparison. The base acceleration is shown in Fig. 9. Results of the surface acceleration and velocity obtained from both methods of analysis are presented in Figs. 10, 11, 12 and 13 for comparison.

From both these test cases it can be seen that the maximum values and the general trend of the surface motion obtained on the basis of the SDF model is in very good agreement with that of the MDF model. However, as should be expected, this conclusion does not hold true for the frequency content of the surface motion, especially that of the surface acceleration.

PRESENTATION OF THE RESULTS

The results of SDF soil layer response computations, in the form of iso-intensity contours of maximum surface velocity and acceleration normalized with respect to the maximum base rock velocity and acceleration, are presented in Figs. 14-21. The results are drawn on a log-log grid of the SDF model parameters: the reference displacement, U_r , and the fundamental small strain frequency of vibration, f_1. On each figure the vertical axis represents the reference displacement in centimeters and the horizontal axis represents the fundamental frequency in Hertz. The range of reference displacements is taken between 0.1 and 100 cm, and the range of frequencies is taken between 0.1 and 10 Hz. For adequate resolution of iso-intensity contours, response computations are carried out at 16 different frequency and 20 different reference displacement points, providing 320 values for each figure. The total CPU time spent for each record is about 10 minutes for 15 seconds of integration duration, using an IBM-370-155 computer.

Four different strong motion records corresponding to the following earthquakes and recording sites are employed as bedrock motions:

a) The first 20 seconds of the N21E component of the Taft record of the 7-21-1952, 0453 PDT, Kern County earthquake with a maximum acceleration, a_{max} , of 0.176 g, a maximum velocity, V_{max}, of 16.95 cm/sec, a maximum displacement, d_{max} , of 8.5 cm, and an initial velocity, V_o, of -1 cm/sec.

b) The first 15 seconds of the N-S component of the El-Centro record of the 5-8-40, 2037 PST Imperial Valley earthquake with a_{max} = 0.347 g, V_{max} = 36.32 cm/sec., d_{max} = 10.01 cm, and V_o = 5.36 cm/sec. (Record: IA 1, 40.1).

c) The first 15 seconds of the S74W component of the Pacoima Dam record of the 2-9-71, 0600 PST San Fernando earthquake with a_{max} = 1.249g, V_{max} = 57.60 cm/sec, d_{max} +13.48 cm, and V_o=-0.11 cm/sec/ (Record: 71.001).

d) The first 15 seconds of the S80E component of the Golden Gate Park record of the 3-22-57, 1144 PST San Francisco earthquake with a_{max} = 0.123 g, V_{max} = 4.48 cm/sec, d_{max} = 0.82 cm, and V_o = 0.16 cm/sec. (Record: 1A 15, 57.6 T).

These records are base line corrected by a method employing least squares straight line adjustment in conjunction with Butterworth 2nd order low-cut digital filtering.

DISCUSSION AND GENERAL CONCLUSIONS

As it can clearly be seen from Figs. 5, 6, 7, 8, 10, 11, 12 and 13, time histories of both the surface acceleration and velocity obtained from the SDF model compare favorably with those obtained from the Multi-Degree-of-Freedom analysis of Joyner (1977). However, it should be noted that this comparison does not hold true for the frequency content of the time histories, since by nature, the SDF model is deficient in the frequency contents higher than the dominant ground frequency.

The range of the maximum, normalized iso-acceleration and iso-velocity contour values are presented in Table 3. These values are associated with the soil layer first frequency range of 0.1 to 10 Hz, and reference displacement range of 0.1 to 100 cm. covering an extensive choice of soil layer types. Scaling is permissible within a given iso-acceleration or iso-velocity contour map. That is, if a given strong motion record is scaled by a factor, the iso-accleration or the iso-velocity contour map corresponding to this scaled strong motion input can be obtained by multiplying the reference displacement values by the same scaling factor and using the map corresponding to the unscaled strong motion.

It can be observed that the iso-acceleration and the iso-velocity contour maps corresponding to different strong motions are quite coherent among themselves and follow the same general trends.

For iso-acceleration maps, the contour curves are generally parallel to each other with contour values increasing with increasing frequency and reference displacement. The contours are also orthogonal to a direction making about 20 degrees with the frequency axis. The most important variable seems to be the frequency and the contour values are only slightly sensitive to the reference displacement except at or near the frequency regions where

the soil fundamental frequency coincide with the dominant ground motion frequency. For iso-velocity maps, although the contours follow the same general trends as of iso-acceleration maps, there is strong dependence to both of the soil frequency and reference displacement parameters. This dependence increases in complexity, especially at or near the frequency regions where the soil fundamental frequency approach to that of the strong ground motion due to resonance effects.

As a conclusion, although these types of approximate studies lack the accuracy associated with the multi-degree-of-freedom analysis, they are valuable tools in assessment of main parameters and, considering the uncertainties involved in probable base rock motion prescription, the approximate SDF method presented can be of value over the more elaborate methods for microzoning and seismic risk evaluations.

ACKNOWLEDGMENTS

This research was carried out during the visit of the author to the USGS on leave from the Earthquake Engineering Research Institute of the Middle East Technical University, Ankara, Turkey. Financial support for the visit was provided by the USGS and the above institute and is gratefully acknowledged.

REFERENCES CITED

Bishop, A. W., I. Alpan, G. E. Blight, and I. B. Donald (1961). Factors controlling the strength of partly saturated cohesive soils, in Research Conference on Shear Strength of Cohesive Soils, ASCE, New York, 503-532.

Cervantes, R., L. Esteva, and G. Alduncin (1973). Riesgo sismico en formaciones estraficadas, Internal Report, Institute of Engineering, National University of Mexico, Mexico City.

Constantopulos, I. V. (1973). Amplification studies for nonlinear hysteretic soil model, Research Report R-70-14, Dept. of Civil Eng., Massachusetts Institute of Technology, Cambridge, Massachusetts.

Crandal, S. H., Engineering Analysis, Mc Graw-Hill Book Co., New York, N. Y., 1956.

Dobry, R. (1970). Damping in Soils: Its hysteretic nature and the linear approximation, Research Report R70-14, Dept. of Civil Eng., Massachusetts Institute of Technology, Cambridge, Massachusetts.

Dobry, R., R. V. Whitman, and J. M. Roesset (1971). Soil properties and the one-dimensional theory of earthquake amplification, Research Report R-71-18, Dept. of Civil Eng., Massachusetts Institute of Technology, Cambridge, Massachusetts.

Dobry. R., I. Oweis, and A. Urzua (1976). Simplified procdures for estimating the fundamental period of a soil profile, Bull. Seism. Soc. Am. 66, 1293-1321.

Erdik, M. O. (1975). Torsional effects in dynamically excited structures, Doctoral Thesis, Dept. of Civil Eng., Rice University, Houston, Texas.

Faccioli, E., E. Santoyo, and J. L. Leon (1973). Microzonation criteria and seismic response studies for the city of Managua, Proc. Conf. Managua,

Nicaragua Earthquake, San Francisco, California, I, 271-291.

Faccioli, E., and J. Ramirez (1976). Earthquake response of nonlinear hysteretic soil systems, Intern. J. Earthquake Eng. Struct. Dynamics, 4, 261-276.

Hardin, B. O., and W. L. Black (1969). Vibration modulus of normally consolidated clay (discussion), Proc. Am. Soc. Civil Eng., J. Soil Mech. Found. Div. 95, 1531-1537.

Hardin, B. O. and V. P. Drnevich (1972a). Shear modulus and damping in soils: Measurement and parameter effects, Proc. Am. Soc. Civil Eng., J. Soil Mech. Found. Div. 98, 603-624.

Hardin, B. O. and V. P. Drnevich (1972b). Shear modulus and damping in soils: Design equations and curves, Proc. Am. Soc. Civil Eng., J. Soil Mech. Found. Div. 98, 667-692.

Hurty, W. C. and M. F. Rubinstein (1964) Dynamics of Structures, Prentice-Hall, Inc., Englewood Cliffs, New Jersey.

Idriss, I. M. and H. B. Seed (1967). Response of Horizontal Soil Layers During Earthquakes, Dept. of Civil Eng., University of California, Berkeley, California.

Idriss, I. M. and H. B. Seed (1968). Seismic Response of Horizontal Soil Layers, Proc. Am. Soc. Civil Eng., J. Soil Mech. Found. Div. 94, 1003-1031.

Joyner, W. B. (1975), A method for calculating nonlinear seismic response in two dimensions, Bull. Seism. Soc. Am. 65, 1337-1357.

Joyner, W. B., and A. T. F. Chen (1975), Calculation of nonlinear ground response in earthquakes, Bull. Seism. Soc. Am. 65, 1315-1336.

Joyner, W. B. (1977), A Fortran Program For Calculating Nonlinear Seismic Ground Response, U. S. Geological Survey, Open File Report 77-671.

Ladd, C. C. and L. Edgers (1972). Consolidated-undrained direct-simple shear

tests on saturated clays, Research Report R-72-82, Dept. of Civil Eng., Massachusetts Institute of Technology, Cambridge, Massachusetts.

Masing, G. (1926). Eigenspannungen und verfestigung beim Messing, Proc. Intern. Congr. Appl. Mech. 332-335.

Newmark, N. M. (1959). A method of computation for structural dynamics, Proc. Am. Soc. Civil Eng., J. Eng. Mech. Div. 85, 67-94.

Newmark, N. M. and E. Rosenblueth (1971). Fundamentals of Earthquake Engineering, Prentice Hall, Inc., Englewood Cliffs, New Jersey.

Papadakis, C. N. (1973). Soil transients by characteristics methods, Doctoral Thesis, Dept. of Civil Eng., University of Michigan, Ann Arbor, Michigan.

Richart, F. E. (1975). Some effects of dynamic soil properties on soil-structure interaction, Proc. Am. Soc. Civil Eng. 101, (GT-12) 1193-1240.

Schnabel, P. B., J. Lysmer, and H. B. Seed (1972). SHAKE, a computer program for earthquake response analysis of horizontally layered sites, Report EERC 72-12, Earthquake Eng. Res. Center, University of California, Berkeley, California.

Seed, H. B. and I. M. Idriss (1969). Influence of soil conditions on ground motions during earthquakes, Proc. Am. Soc. Civil Eng. (SM-1) 95, 99-137.

Stodola, A., Steam and Gas Turbines, Translated by L. C. Lowenstein, Vols. 1 and 2, McGraw Hill, Inc., New York, N. Y., 1927.

TABLE 1

$\frac{u_o}{U_r}$	$\frac{E_{soil}}{U_r \bar{\tau}_{max}}$
0	0
0.25	0.017
0.5	0.105
1	0.556
2	2.374
5	11.602
10	31.597
20	76.701
50	221.846

TABLE 2

$\frac{y}{U_r}$	$\frac{E_{SDF}}{U_r \cdot \bar{\tau}_{max}}$
0	0
0.25	0.019
0.5	0.115
1	0.575
2	2.328
5	10.899
10	29.240
20	70.472
50	202.995

TABLE 3

Strong Motion and the Associated Max. Acc.	Range of Iso-Acc. Values	Frequency at which Max. Iso-Acc. Occurs
Taft, 0.176g	0.002 - 7.0	7.0 Hz.
El-Centro, 0.347g	0.002 - 6.0	6.0 Hz.
Pacoima, 1.249g	0.0005- 4.0	7.0 Hz.
Golden Gate, 0.123g	0.002 - 9.0	7.0 Hz.

Strong Motion and the Associated Max. Vel.	Range of Iso-Vel Values	Frequency at which Max. Iso-Vel. Occurs
Taft, 16.95 cm/sec	0.1 - 3.5	2.0 Hz.
El-Centro, 36.32 cm/sec	0.1 - 3.0	3.0 Hz.
Pacoima, 57.60 cm/sec	0.1 - 4.0	4.0 Hz.
Golden Gate, 4.48 cm/sec	0.2 - 4.0	4.0 Hz.

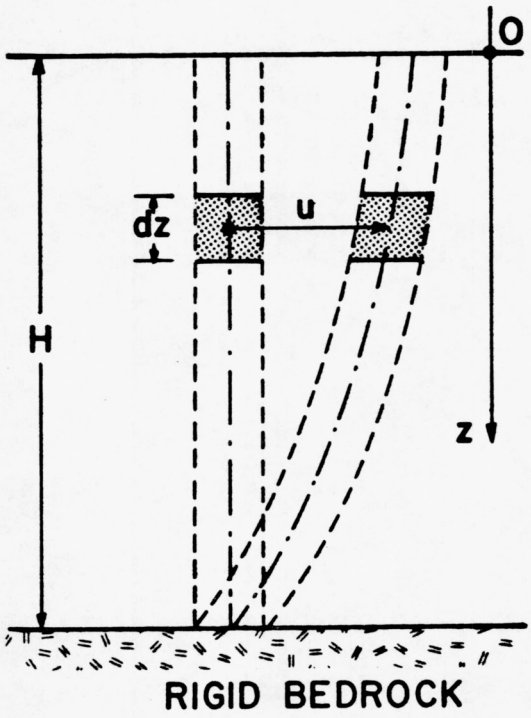

Figure 1.

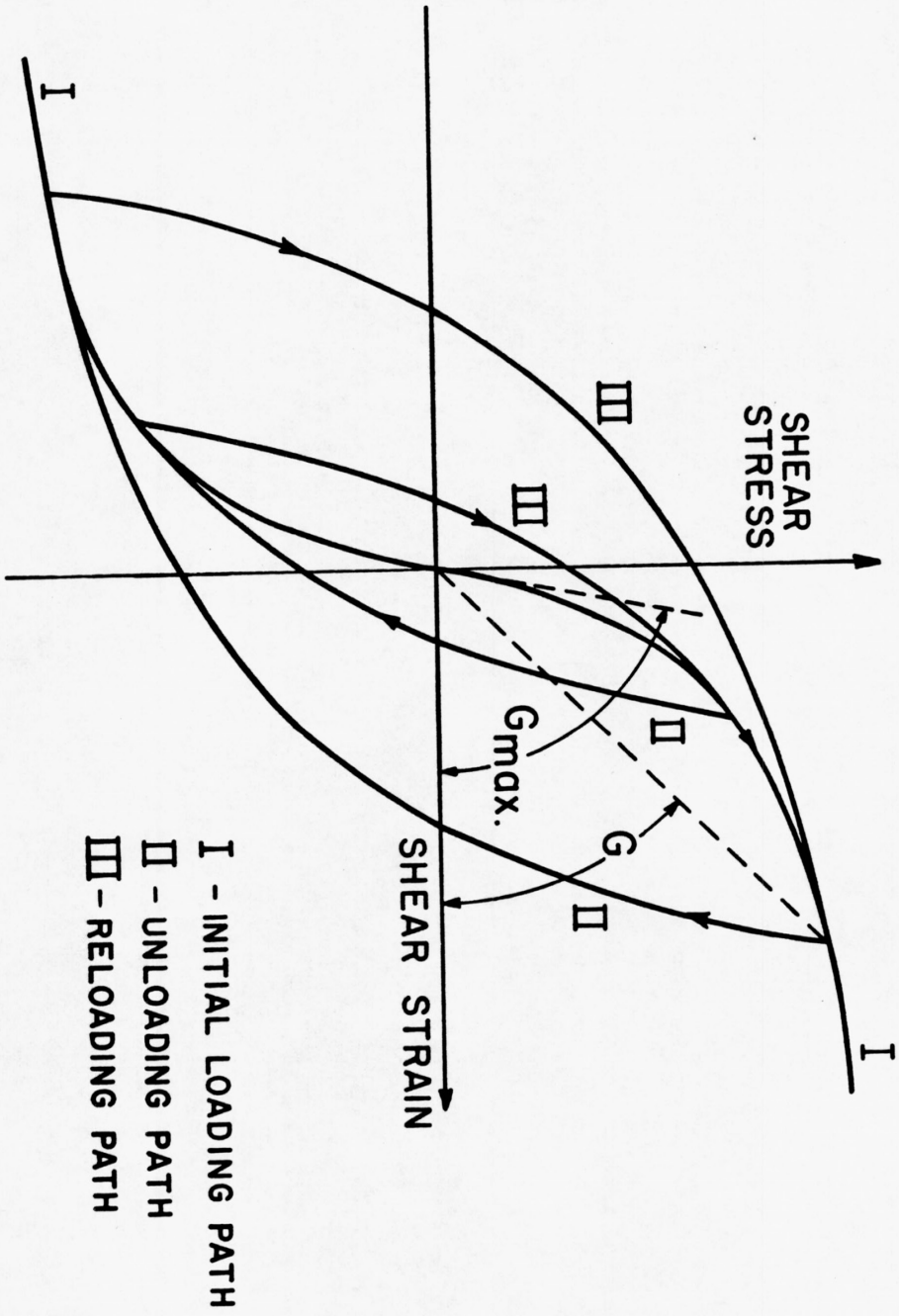
SHEAR STRESS
SHEAR STRAIN
I
II
III
III
II
I
Gmax.
G
I - INITIAL LOADING PATH
II - UNLOADING PATH
III - RELOADING PATH

Figure 2.

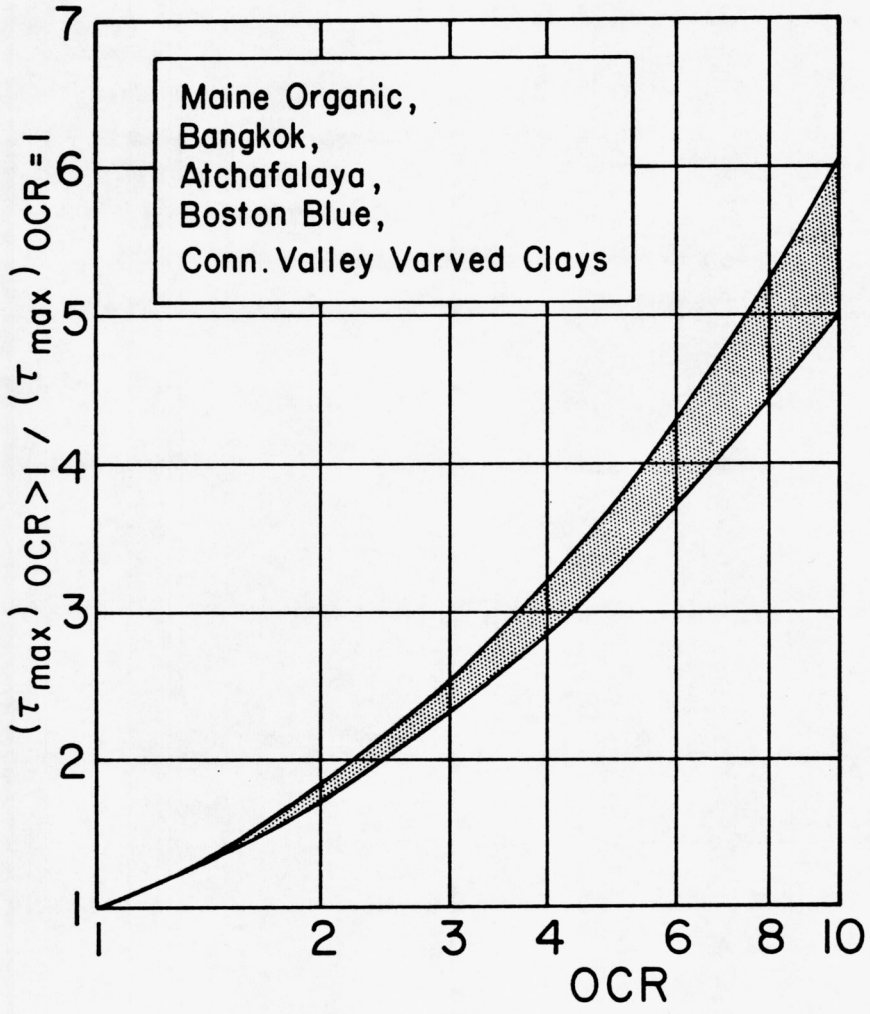
Maine Organic,
Bangkok,
Atchafalaya,
Boston Blue,
Conn. Valley Varved Clays
$(\tau_{max})_{OCR>1} / (\tau_{max})_{OCR=1}$
1
2
3
4
5
6
7
1
2
3
4
6
8
10
OCR

Figure 3.

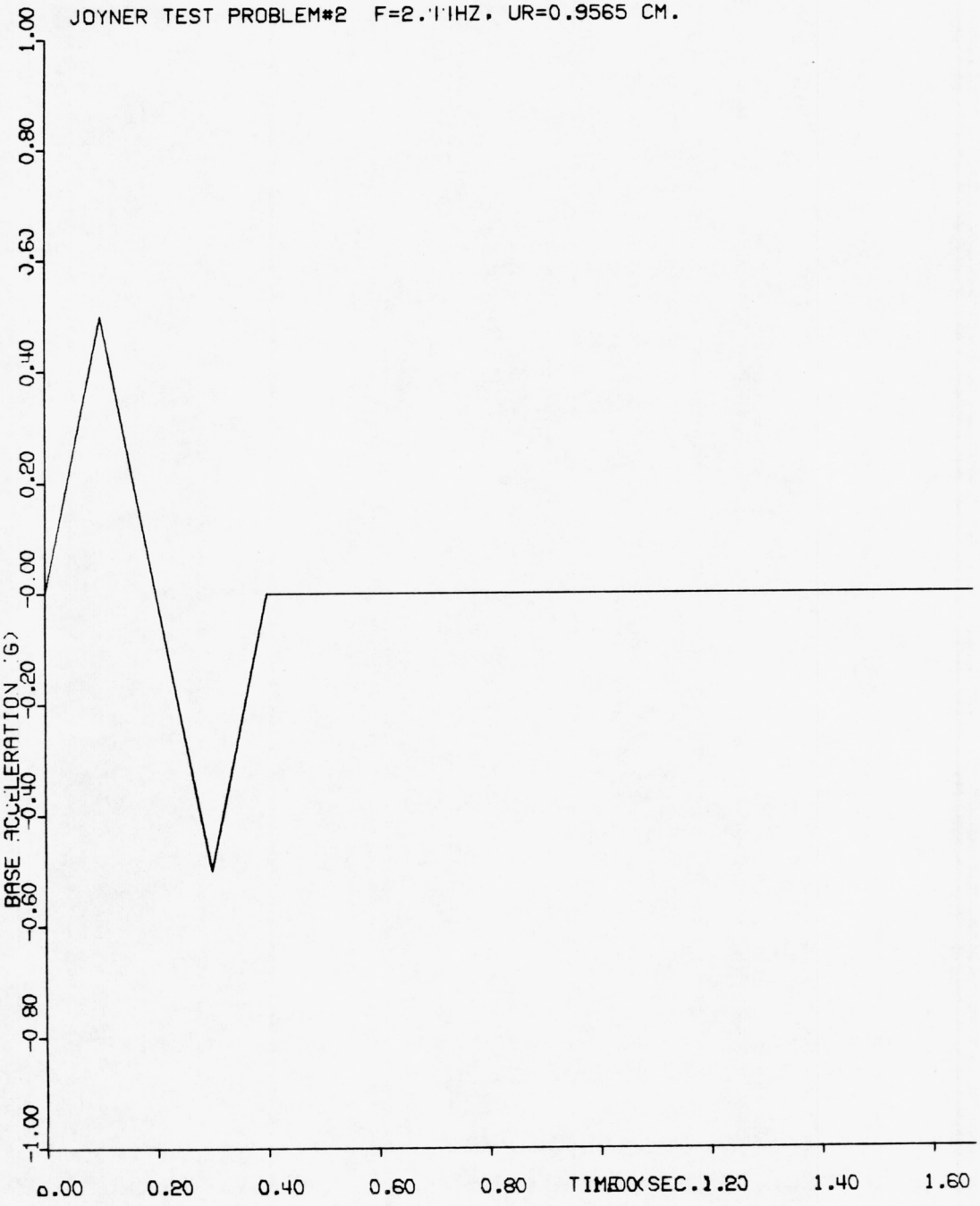

Figure 4. Input acceleration for the first test case.

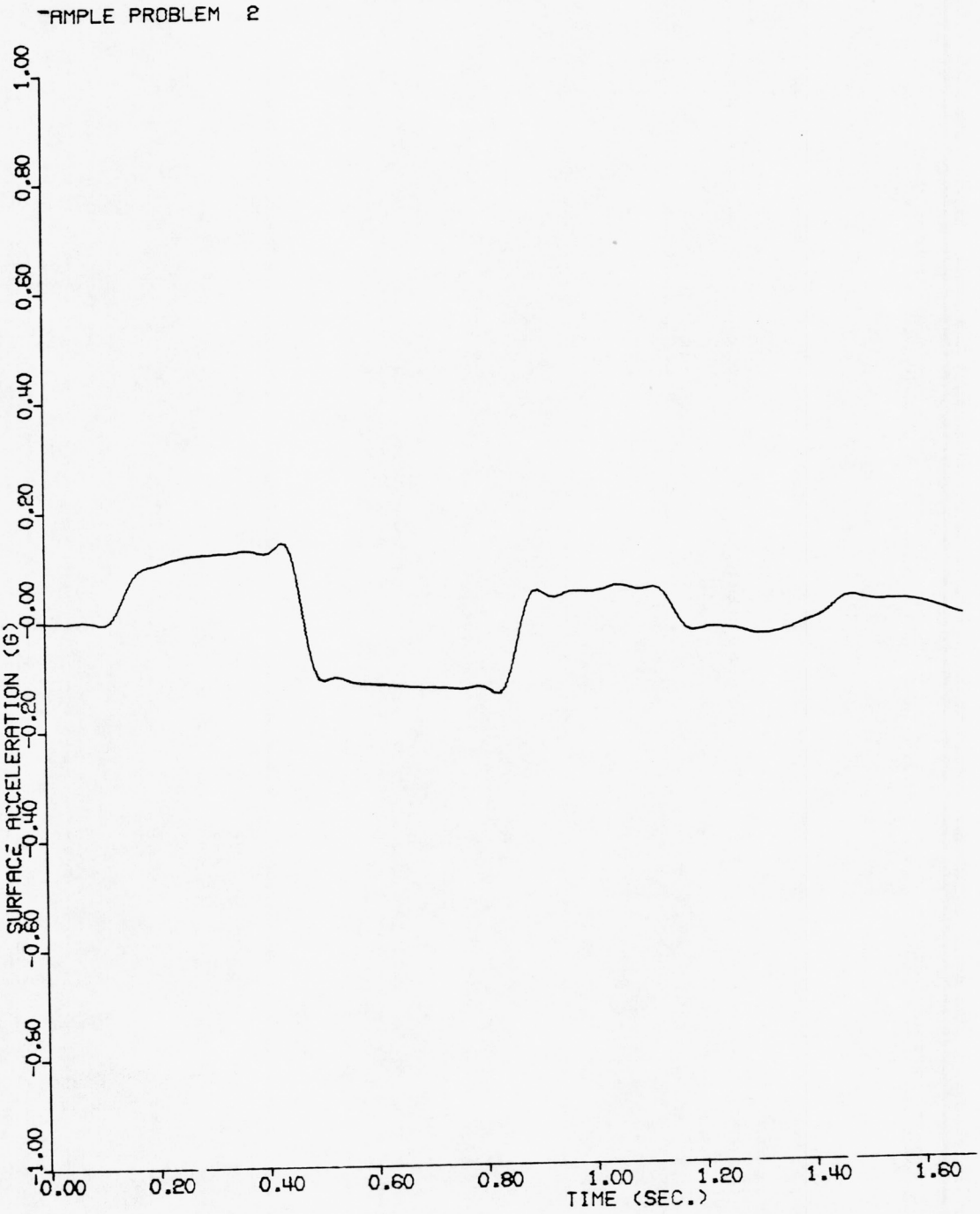

Figure 5. Surface acceleration for the first test case (MDF model).

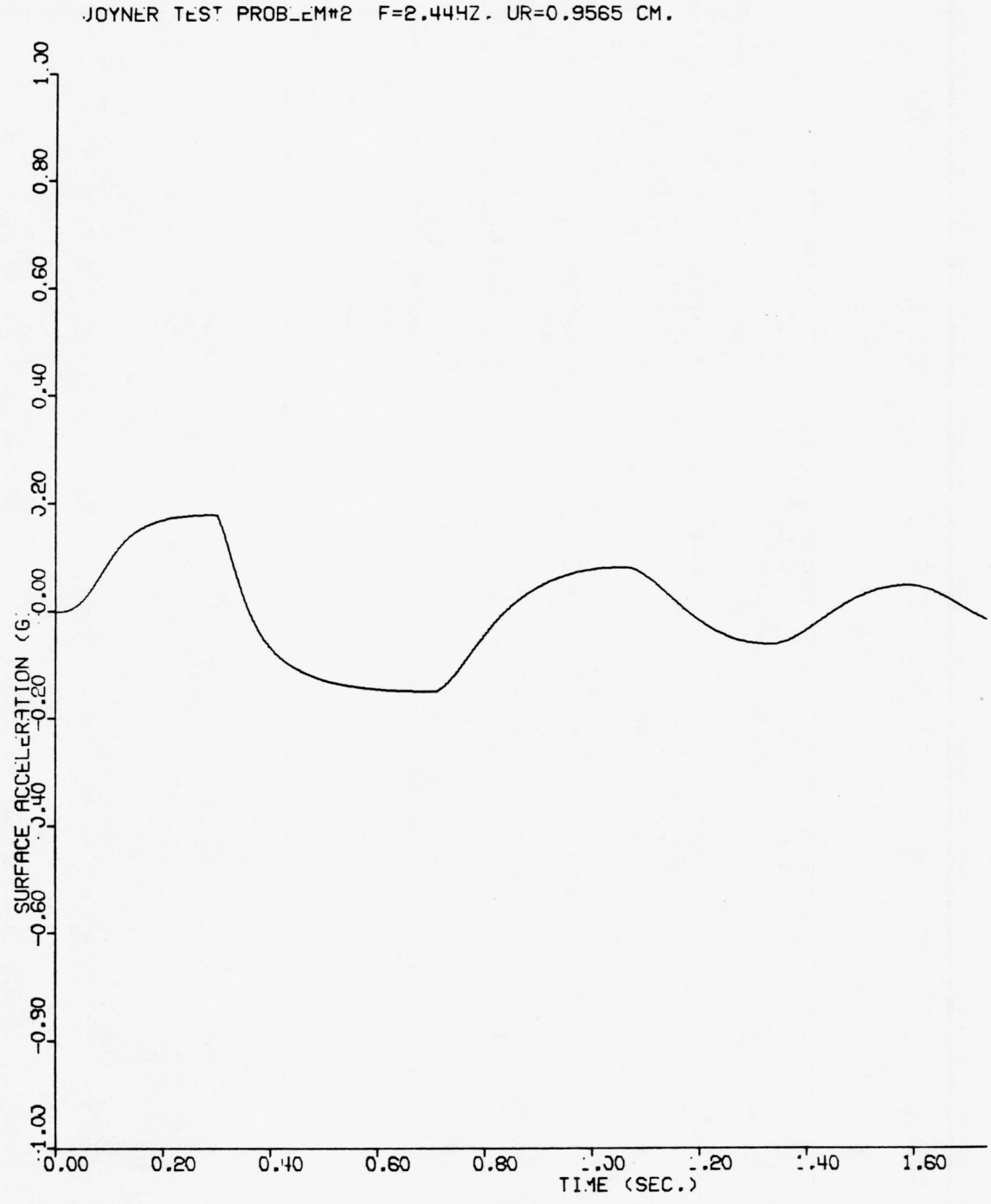

Figure 6. Surface acceleration for the first test case (SDF model).

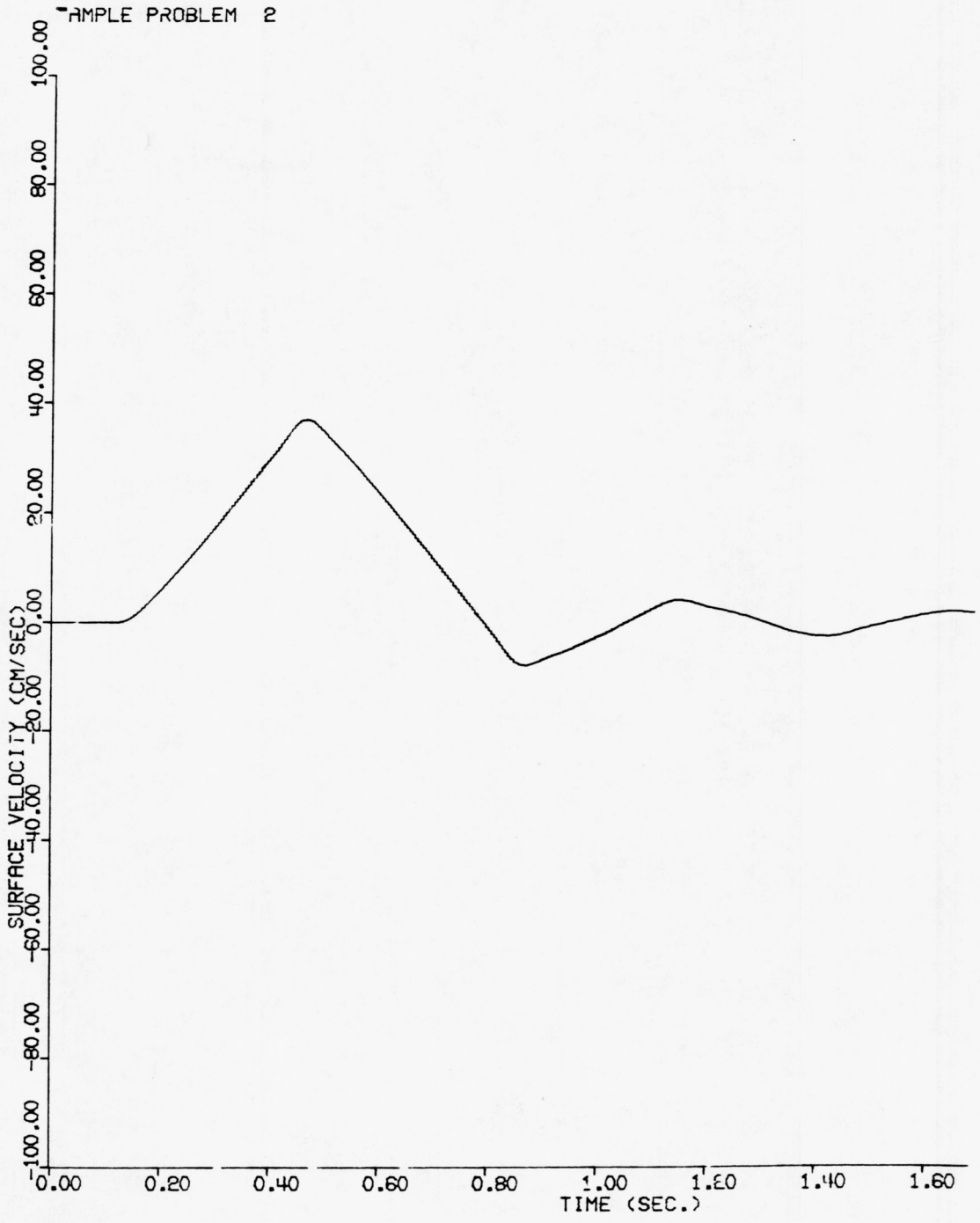

Figure 7. Surface velocity for the first test case (MDF model).

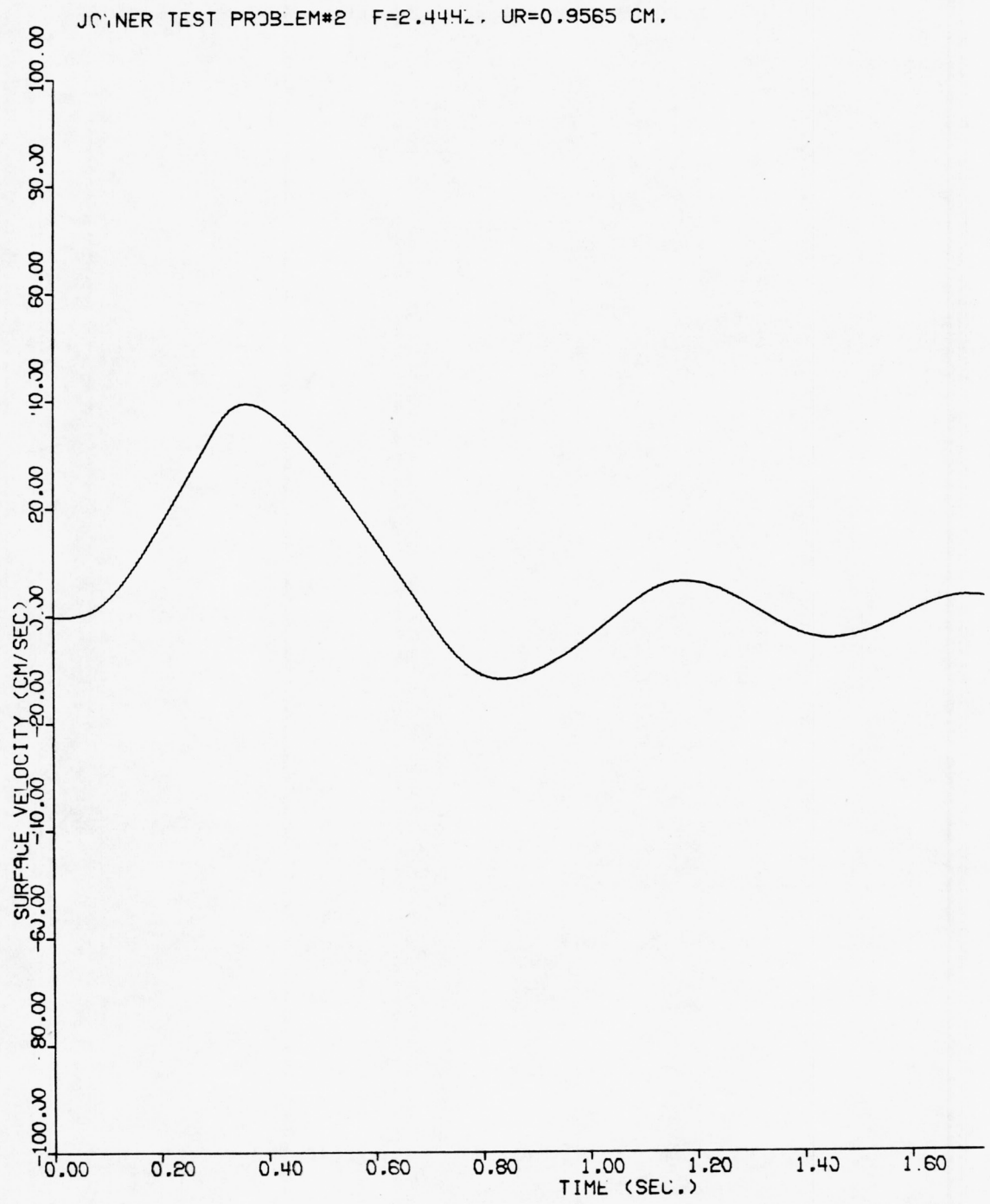

Figure 8. Surface velocity for the first test case (SDF model).

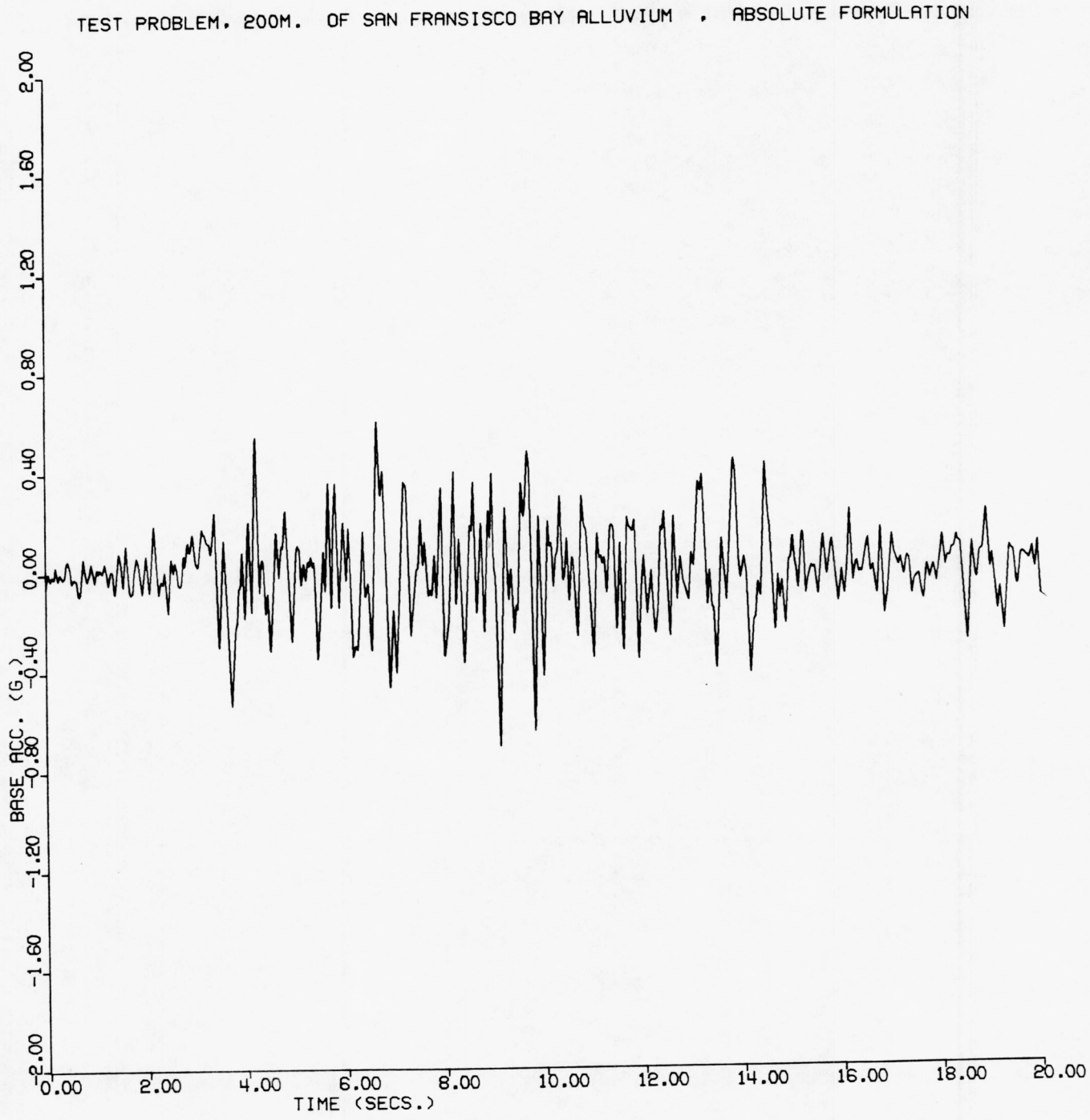

Figure 9. First 20 seconds of the modified Taft strong motion record for the second test case.

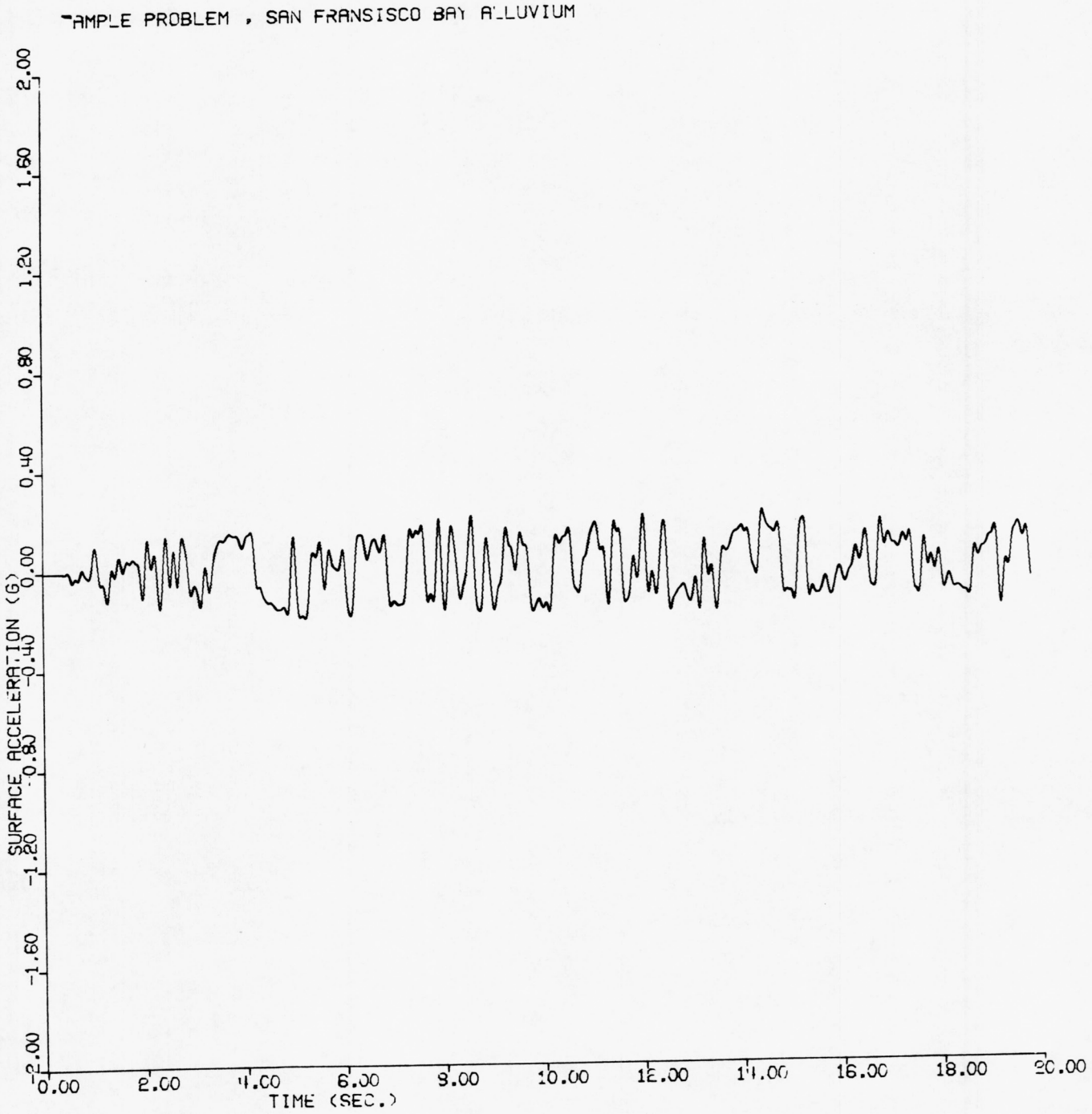

Figure 10. Surface acceleration for the second test case (MDF model).

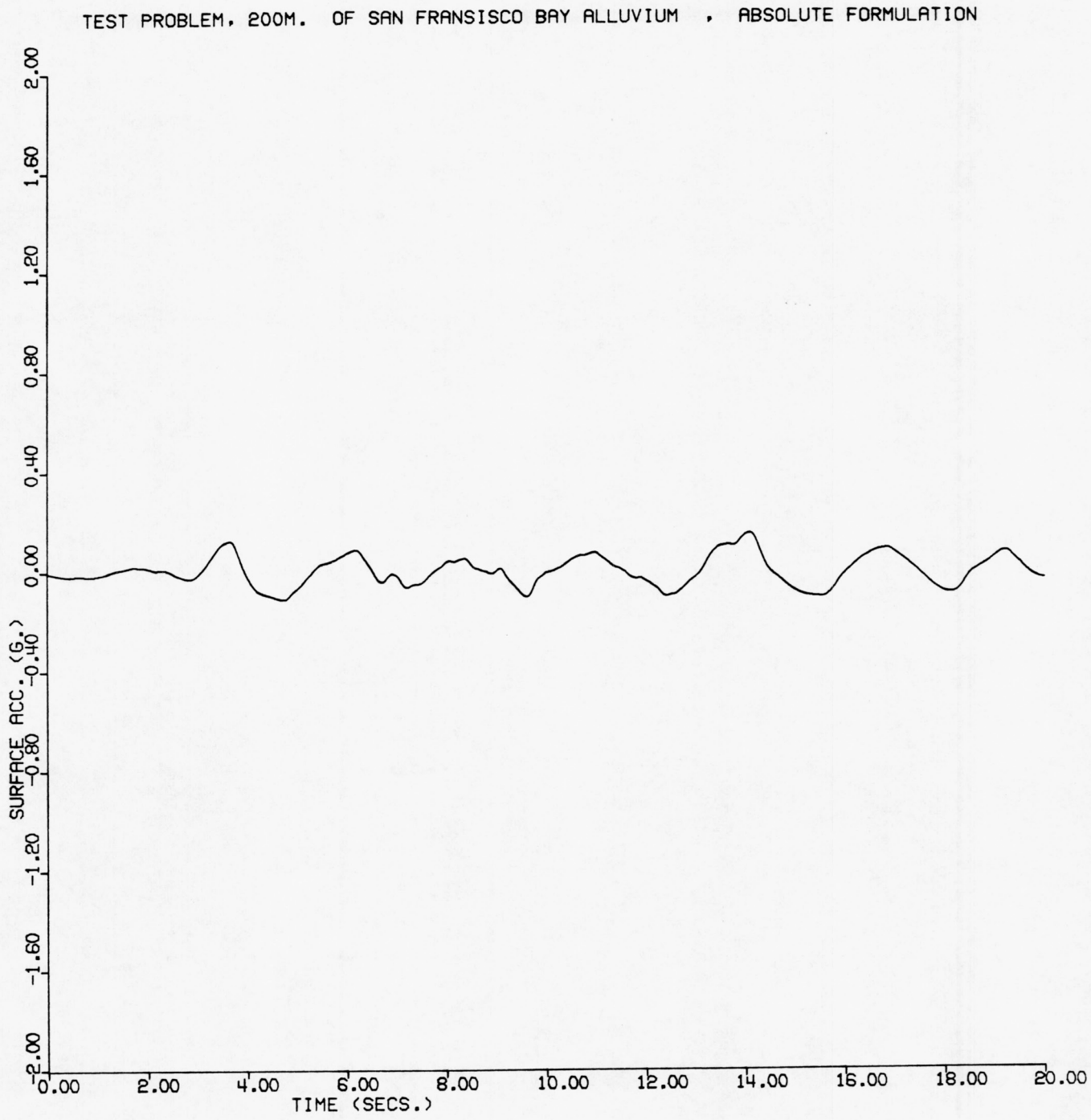

Figure 11. Surface acceleration for the second test case (SDF model).

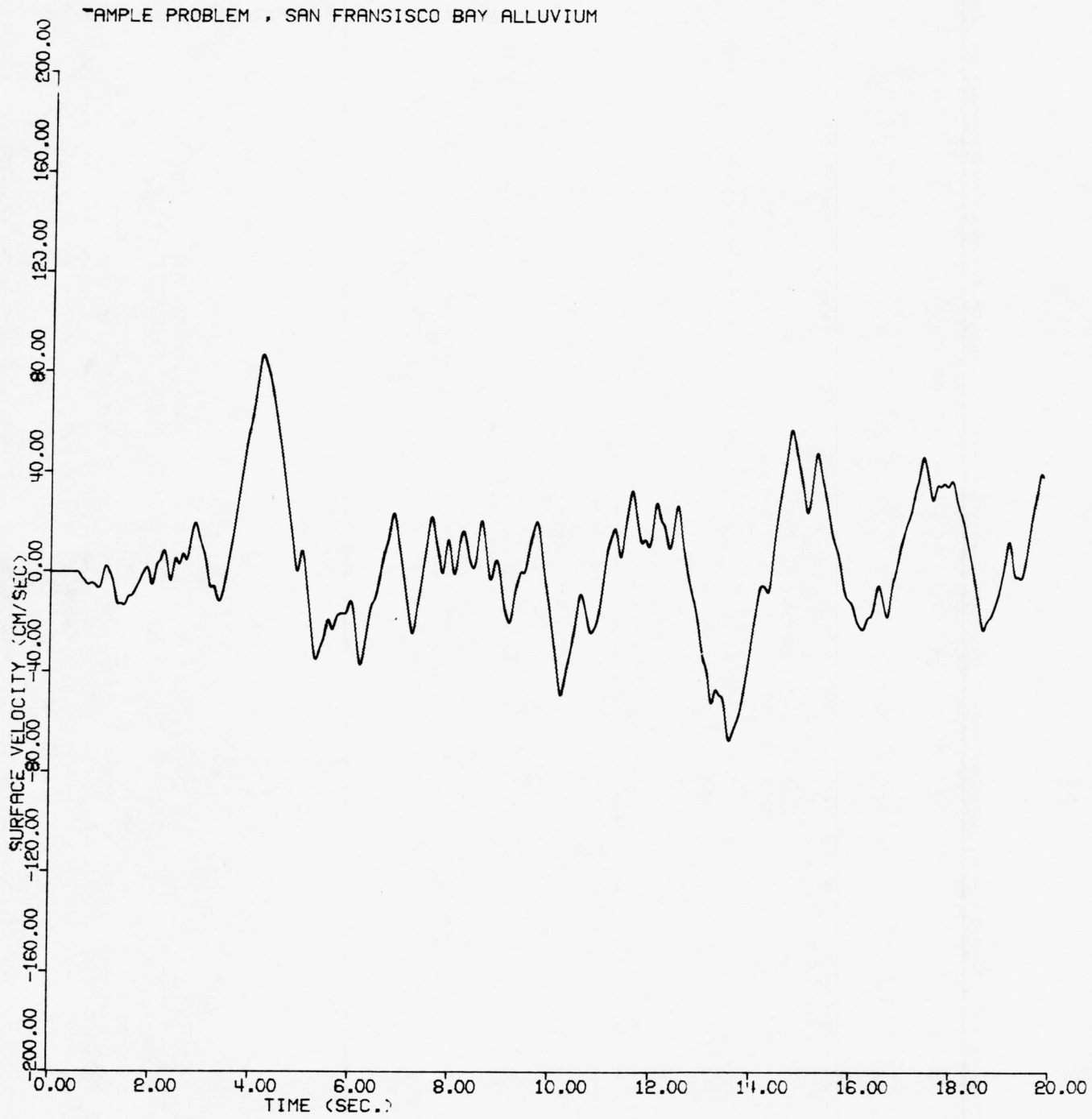

Figure 12. Surface velocity for the second test case (MDF model).

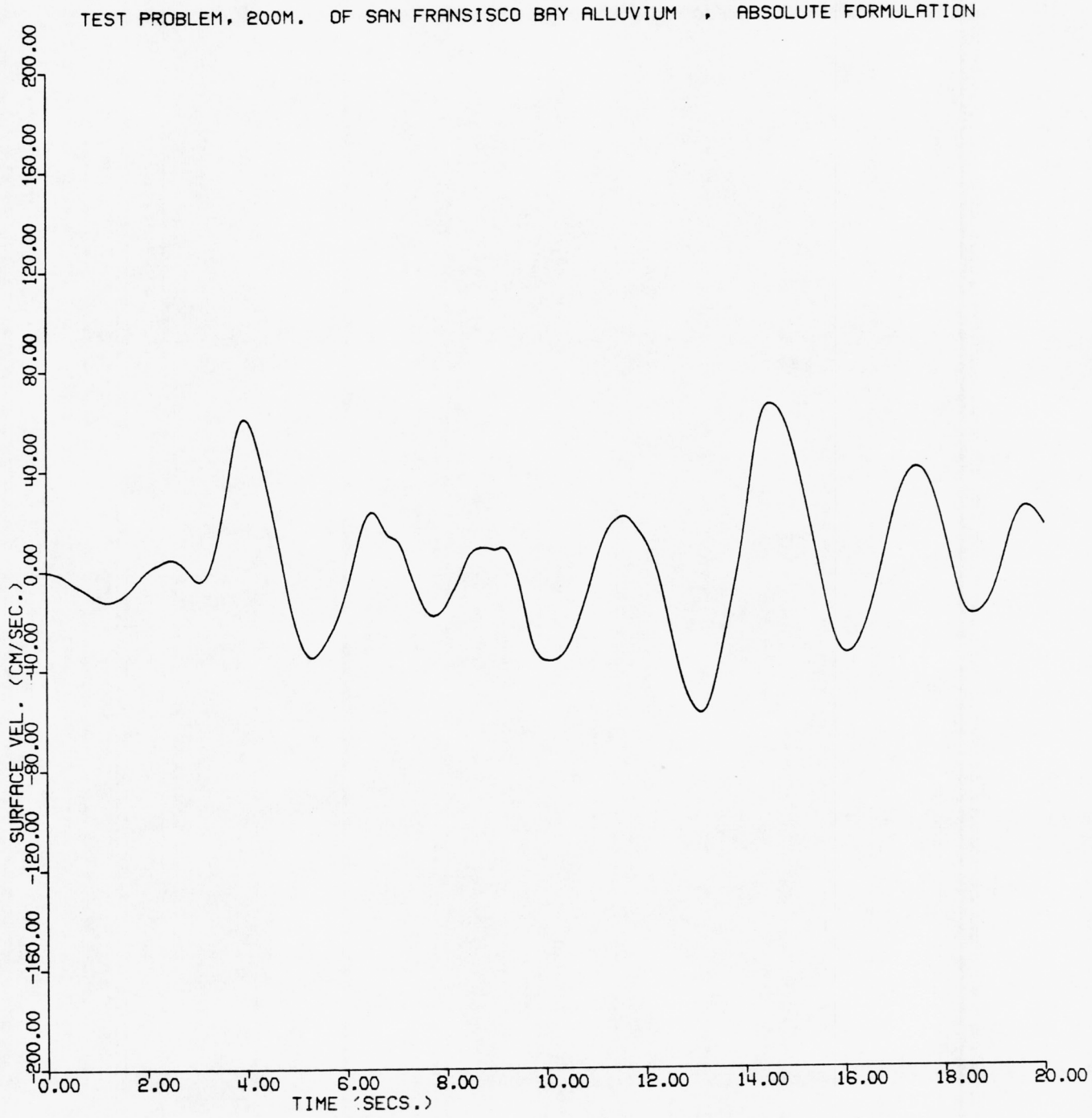

Figure 13. Surface velocity for the second test case (SDF model).

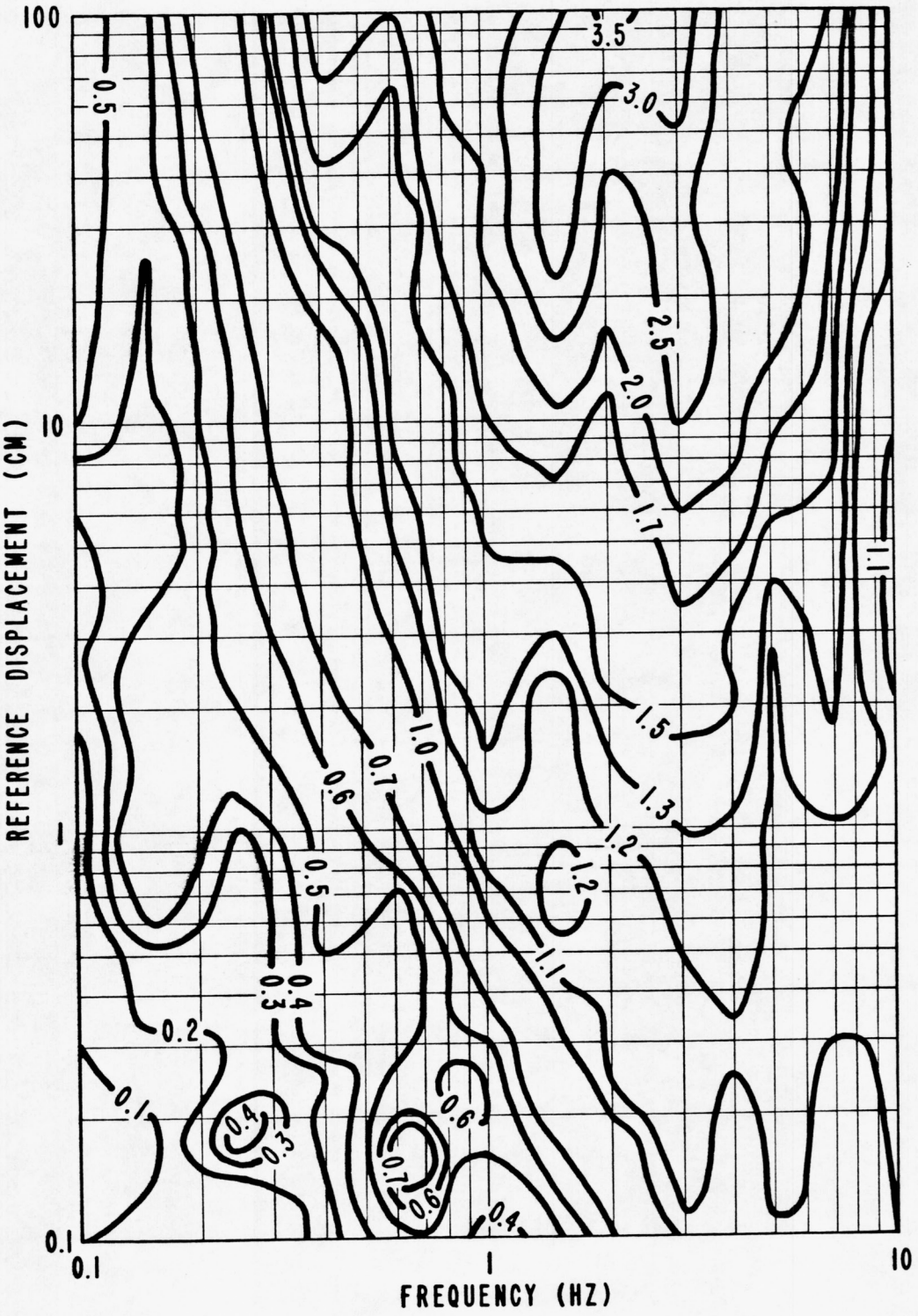

Figure 14. Normalized maximum surface velocity for Taft input.

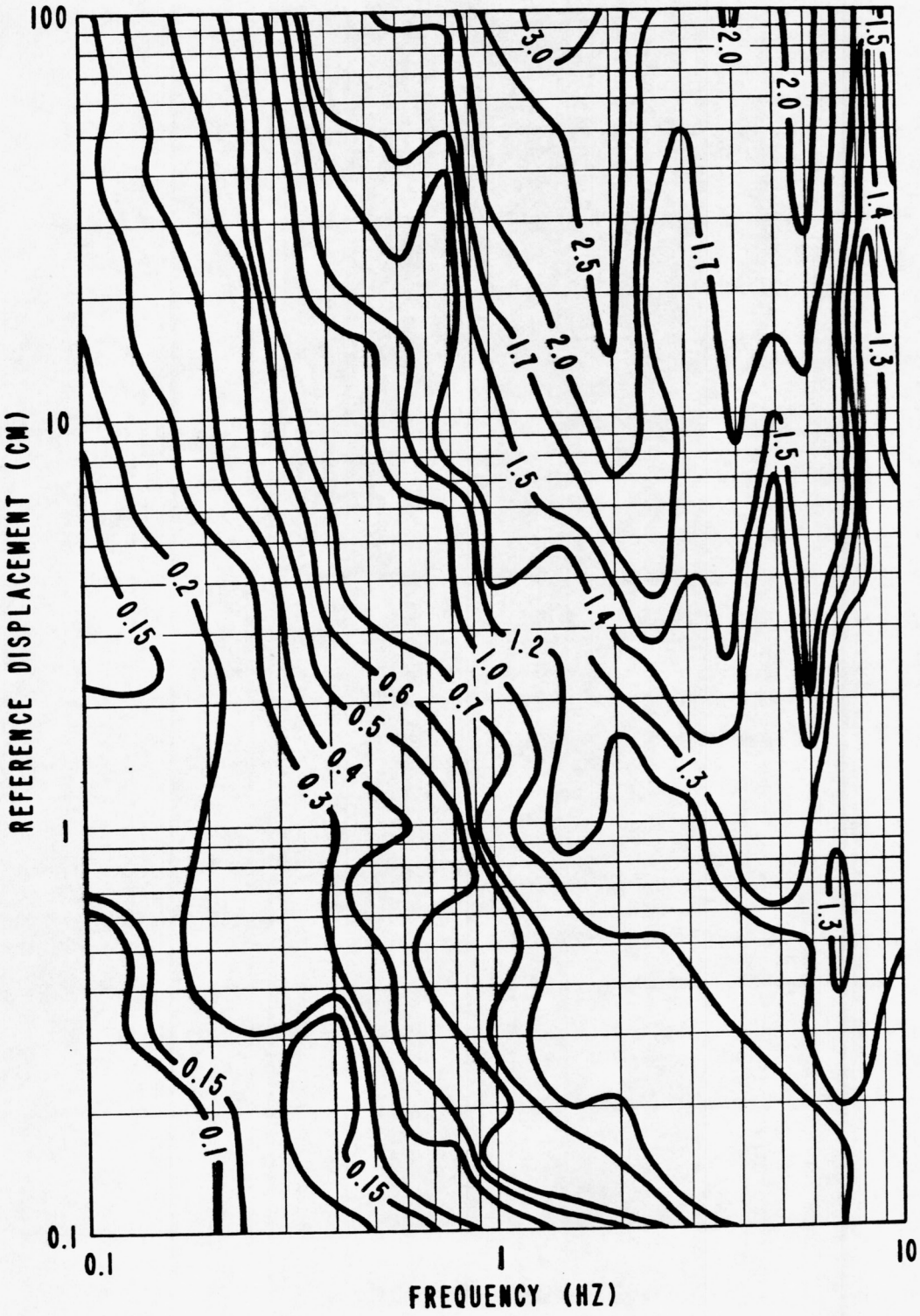

Figure 15. Normalized maximum surface velocity for El Centro input.

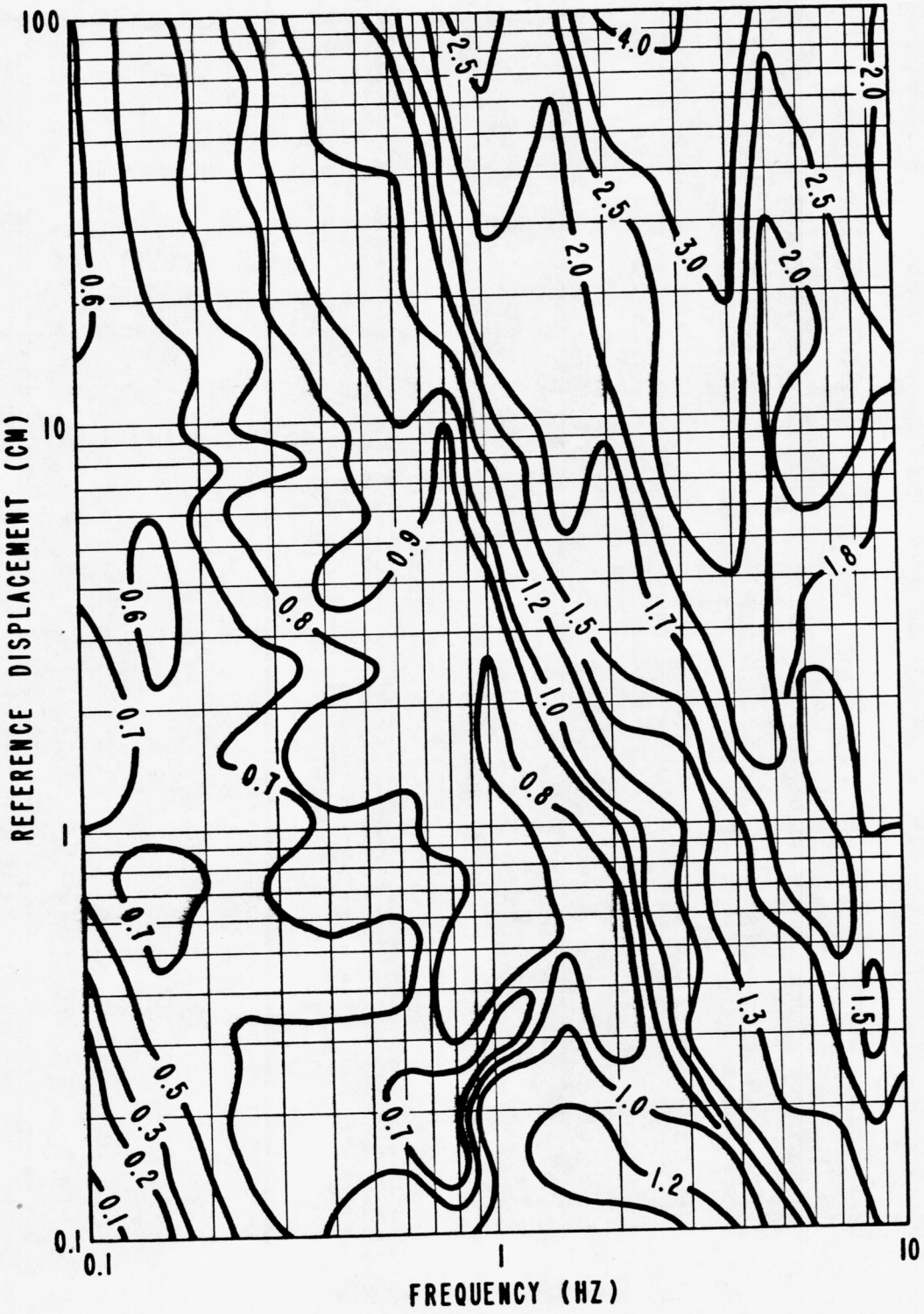

Figure 16. Normalized maximum surface velocity for Pacoima input.

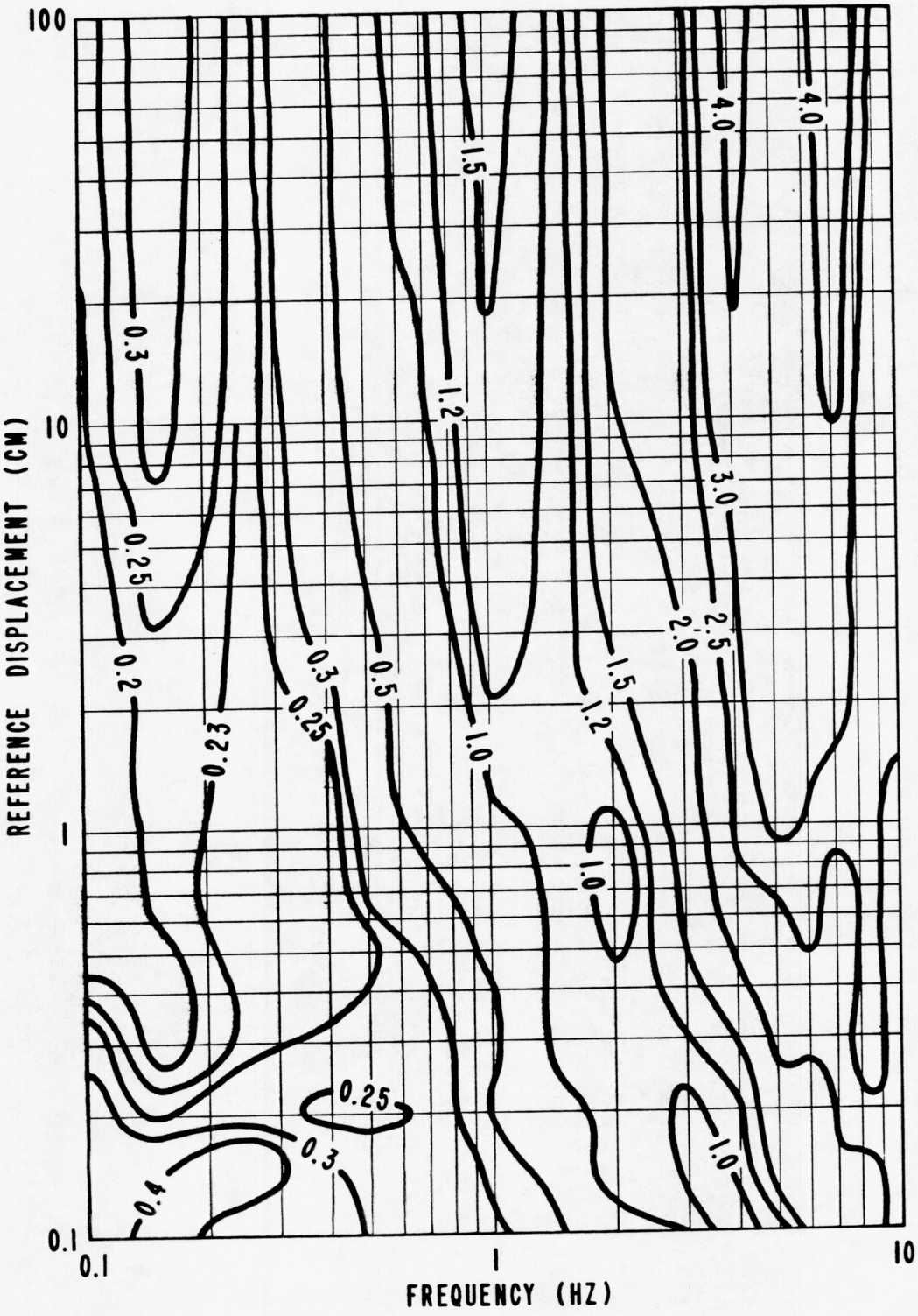

Figure 17. Normalized maximum surface velocity for Golden Gate Park input.

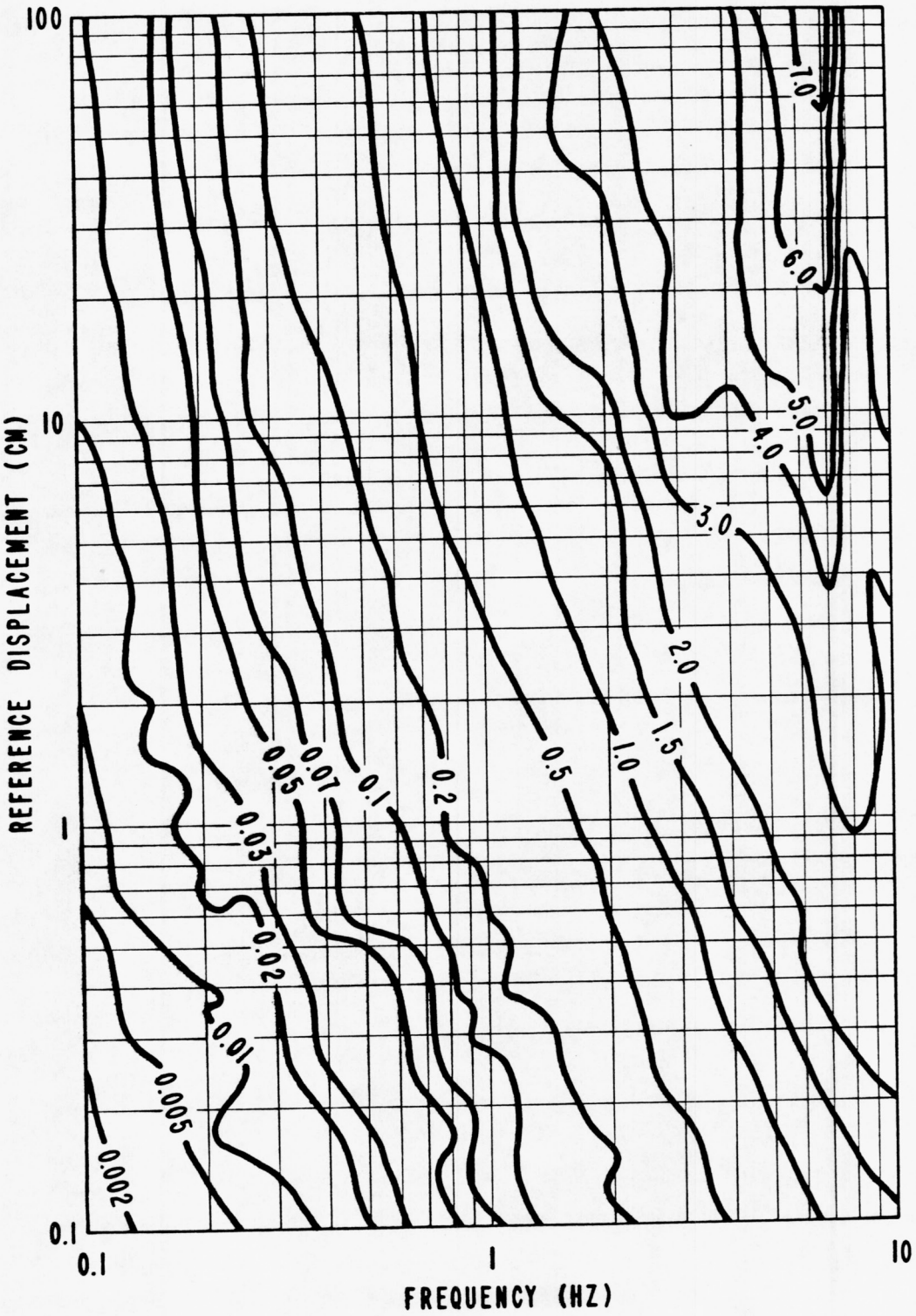

Figure 18. Normalized maximum surface acceleration for Taft input.

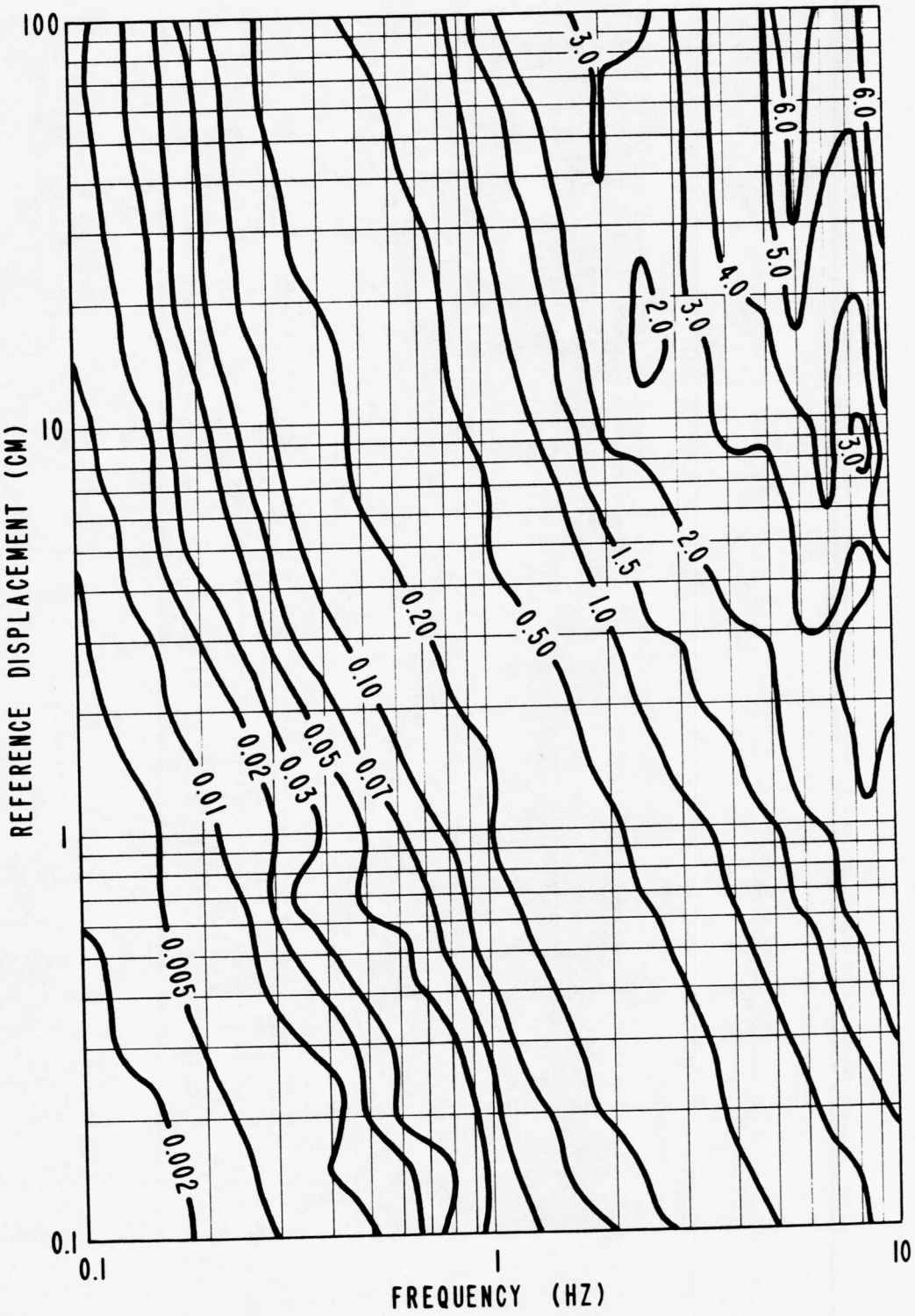

Figure 19. Normalized maximum surface acceleration for El Centro input.

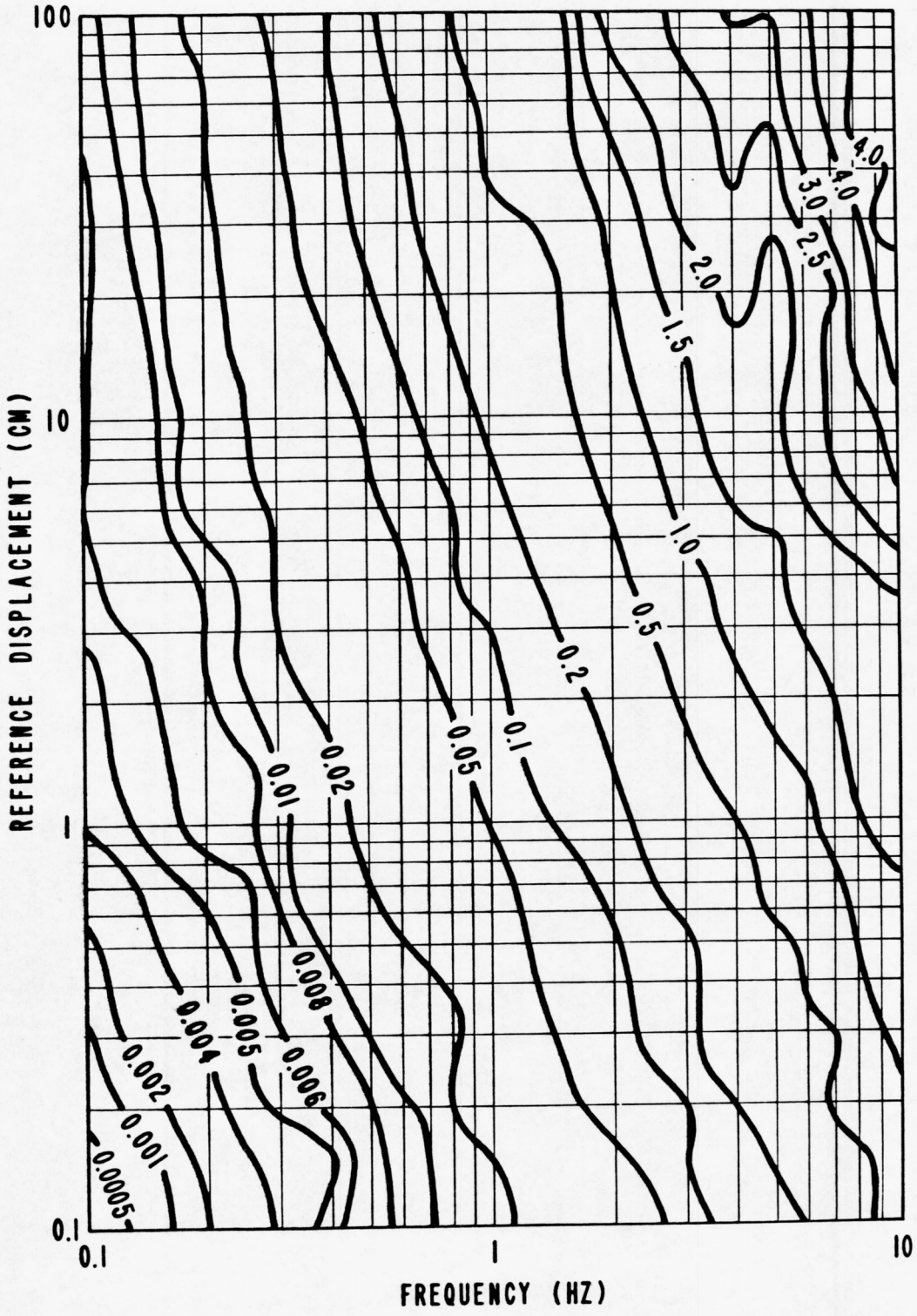

Figure 20. Normalized maximum surface acceleration for Pacoima input.

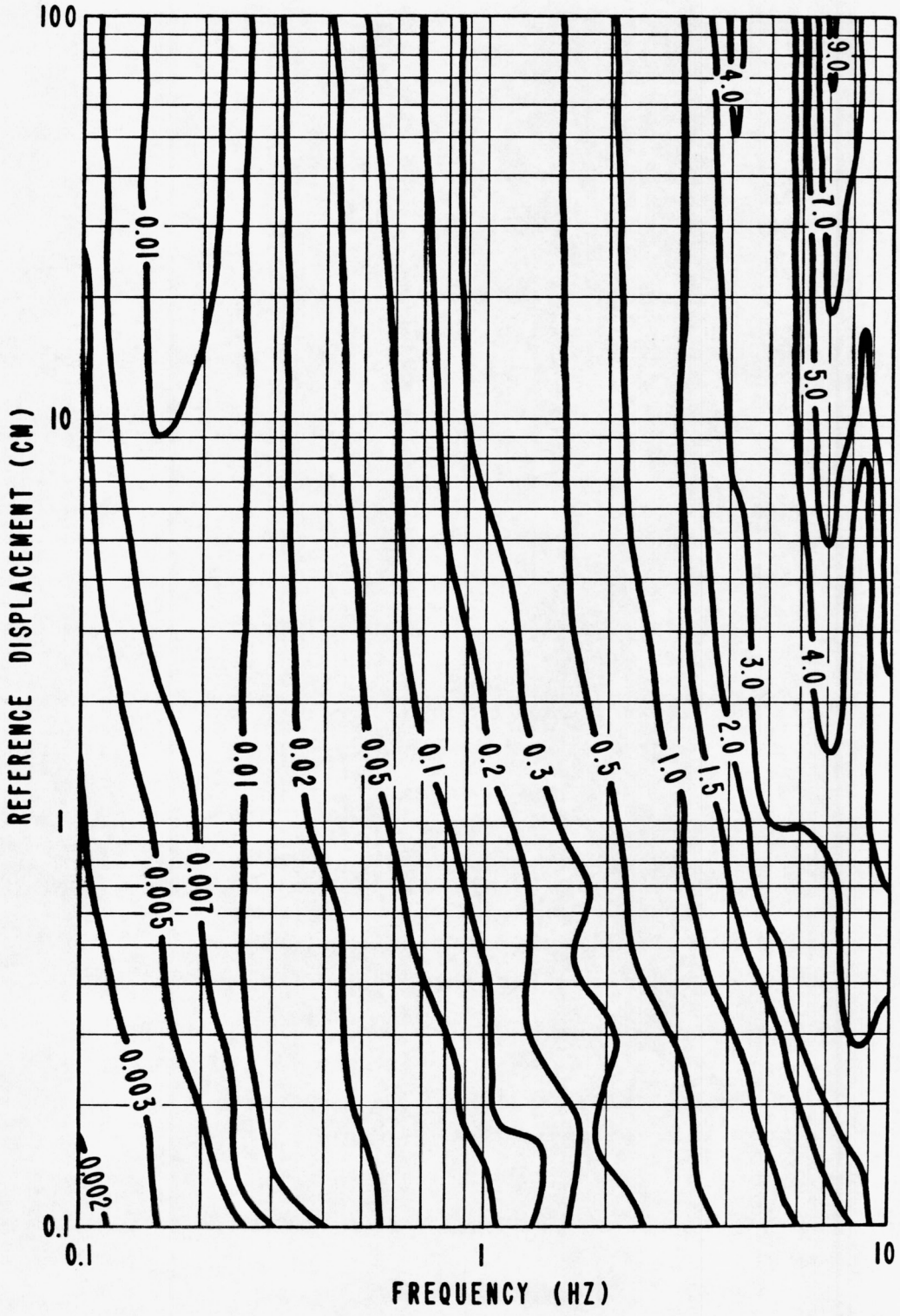

Figure 21. Normalized maximum surface acceleration for Golden Gate Park input.